https://doi.org/10.5194/tc-2021-319
Preprint. Discussion started: 30 November 2021

The Cryosphere Discussions
Open Access
EGU

Review article: Parameterizations of snow-related physical processes in land surface models

Won Young Lee[1,3], Hyeon-Ju Gim[2], and Seon Ki Park[1,3,4,*]

[1]Severe Storm Research Center, Ewha Womans University, Seoul, Republic of Korea
[2]Korea Institute of Atmospheric Prediction Systems, Seoul, Republic of Korea
[3]Center for Climate/Environment Change Prediction Research (CCCPR), Ewha Womans University, Seoul, Republic of Korea
[4]Dept. of Climate Energy Systems Eng., Ewha Womans University, Seoul, Republic of Korea

Correspondence: Seon Ki Park (spark@ewha.ac.kr)

Abstract. Snow on land surface plays a vital role in the interaction between land and atmosphere in the state-of-the-art land surface models (LSMs) and the real world. Since the snow cover affects the snow albedo and the ground and soil heat fluxes, it is crucial to detect snow cover changes accurately. It is challenging to acquire observation data for snow cover, snow albedo, and snow depth; thus, an excellent alternative is to use the simulation data produced by the LSMs that calculate the snow-related physical processes. The LSMs show significant differences in the complexities of the snow parameterizations in terms of variables and processes considered. Thus, the synthetic intercomparisons of the snow physics in the LSMs will help the improvement of each LSM. This study revealed and discussed the differences in the parameterizations among LSMs related to snow cover fraction, snow albedo, and snow density. We selected the most popular and well-documented LSMs embedded in the Earth System Model or operational forecasting systems. We examined single layer schemes, including the Unified Noah Land Surface Model (Noah LSM), the Hydrology Tiled ECMWF Scheme of Surface Exchanges over Land (HTESSEL), the Biosphere-Atmosphere Transfer Scheme (BATS), the Canadian Land Surface Scheme (CLASS), and multilayer schemes of intermediate complexity including the Community Noah Land Surface Model with Multi-Parameterization Options (Noah-MP), the Community Land Model version 5 (CLM 5), the Joint UK Land Environment Simulator (JULES), and the Interaction Soil-Biosphere-Atmosphere (ISBA). First, we identified that BATS, Noah-MP, JULES, and ISBA reflect the snow depth and roughness length to parameterize snow cover fraction, and CLM 5 accounts for the standard deviation of the elevation value for the snow cover decay function. Second, CLM 5 and BATS are relatively complex, so that they explicitly take into account the solar zenith angle, black carbon, mineral dust, organic carbon, and ice grain size for the determinations of snow albedo. Besides, JULES and ISBA are also complicated model which concerns ice grain size, solar zenith angle, new snow depth, fresh snowfall rate, and surface temperature for the albedo scheme. Third, HTESSEL, CLM 5, and ISBA considered the effects of both wind and temperature in the determinations of the new snow density. Especially, ISBA and JULES considered internal snow characteristics such as snow viscosity, snow temperature, and vertical stress for parameterizing new snow density. The future outlook discussed geomorphic and vegetation-related variables for the further improvement of the LSMs. Previous studies clearly show that spatio-temporal variation of snow is due to the influence of altitude, slope, and vegetation condition. Therefore, we recommended applying geomorphic and vegetation factors such as elevation, slope, time-varying roughness

https://doi.org/10.5194/tc-2021-319
Preprint. Discussion started: 30 November 2021


The Cryosphere Discussions

length, vegetation indexes, or optimized parameters according to the land surface type to parameterize snow-related physical processes.

1 Introduction

Physical processes related to snow play an essential role in interacting with the heat and moisture flux between the atmosphere and the land surface and between the land surface and soil. The snow's spatial and temporal heterogeneity causes difficulties in observation, understanding, and modeling (Webster et al., 2018). Changes in snow cover and snow albedo are challenging to measure directly from the ground observation system. Moreover, snow depth is not easy to measure spatially. Therefore, Hedrick et al. (2015) used regional-scale lidar-derived measurements, Fernandes et al. (2018) measured the change of snowpack using lightweight unoccupied vehicle videos, and López-Moreno et al. (2011) discussed sampling strategies and average depth measurements related to snow depth data acquisition. Various land surface models (LSMs) have the advantage of grasping changes in snow elements through modeling variables related to snow because ground observation cannot directly measure these snow elements.

Snow cover plays a vital role in surface albedo, which leads to the exchange of energy and water flux between land and atmosphere. If the snow cover fractions are estimated lower, the land surface albedo will be underestimated (Roesch et al., 2001). In the spring, when solar radiation is at its most intense, snow cover significantly affects the global radiation balance, and snow cover change significantly impacts nature and human systems. Snow is a crucial water source in rivers and groundwater, and it is a more critical resource especially in semi-arid regions (Armstrong and Brun, 2008). Since snow cover is valuable for use as a leisure and travel resource in mid-latitude mountainous regions, it is crucial to monitor snow cover changes accurately. Besides, snow albedo is an important physical property that causes energy interactions between the land surface and the atmosphere, along with the thermal barrier properties of snow and the possibility of phase changes due to latent heat (Armstrong and Brun, 2008). In particular, albedo—the reflectivity of the ground during incident solar radiation—is vital for the land surface's energy balance (Warren and Wiscombe, 1981). Wiscombe and Warren (1980) and Warren and Wiscombe (1980) created early models of snow albedo, and Zhong et al. (2017) improved the snow albedo simulation. Since snow depth is a concept that directly expresses the amount of snowfall, it is imperative to predict or observe accurately to prevent accidents caused by snow. Snow causes delays for both ground and air traffic and heavy snow disasters for crops and livestock. In addition, it causes accidents, injuries, and deaths due to snowfall or snow avalanches (Armstrong and Brun, 2008). Therefore, LSM's parameterization method to determine snow depth using other atmospheric variables as input variables can be essential information to prevent snow-related disasters in areas with no observed snow depth.

As a result of analyzing previous studies, there were studies related to model development or improvement for one or two LSM models. For example, there were snow cover studies (Brun et al., 1992; Yang et al., 1997; Roesch et al., 2001; Brown et al., 2006; Roesch and Roeckner, 2006; Brun et al., 2008; Dutra et al., 2009; Ma et al., 2019), and snow albedo studies (Roesch and Roeckner, 2006; Mölders et al., 2007; Dutra et al., 2009; Wang and Zeng, 2010; Malik et al., 2014; Bartlett and Verseghy, 2015; Zhong et al., 2017; Wang et al., 2020), and studies related to snow depth (Gottlib, 1980; Longley, 1960; Dutra

https://doi.org/10.5194/tc-2021-319
Preprint. Discussion started: 30 November 2021

et al., 2009; Dawson et al., 2017). As a study that directly compared the snow model, Pedersen and Winther (2005) compared and verified the snow albedo parameterization method, and Voordendag et al. (2021) mainly made a simulation comparison of the snow depth change and sublimation process. Mott et al. (2018) reviewed seasonal changes in wind-induced snow cover at three different scales. He et al. (2020) conducted a review on the possibility of improvement by comparing models, including the land surface model for soil thermal conductivity parameterization schemes.

Large-scale projects that conducted model comparison experiments on snow include the Program for Intercomparison of Land-Surface Parameterization Schemes (PILPS) Phase 2d (Pitman and Henderson-Sellers, 1998; Slater et al., 2001), Phase 2e (Bowling et al., 2003), Phase 1 of the Snow Model Intercomparison Project (SnowMIP1; Etchevers et al., 2004), and Phase 2 (SnowMIP2; Essery et al., 2009; Rutter et al., 2009). These projects have shown that large errors occur in warmer winters or warmer regions concerning the time of snow melting in the simulation of snow cover changes (Krinner et al., 2018). In addition, they suggested that more temporal and spatial data could improve their understanding of the snow model and reduce uncertainty about the climate feedback process (Menard et al., 2021). The Earth System Model–Snow Model Intercomparison Project (ESM-SnowMIP; Krinner et al., 2018) is an extension of the Land Surface, Snow and Soil Moisture Model Intercomparison Project (LS3MIP; van den Hurk et al., 2016) at a local scale. The aim was to evaluate snow models and quantify snow-related climate feedback (Krinner et al., 2018). Menard et al. (2021) compared 27 models of ESM-SnowMIP and compared the model ranking through the Normalized Root Mean Square Error (NRMSE) of Snow Water Equivalent (SWE) and surface temperature and the bias of SWE, surface temperature, albedo, and soil temperature.

Although the above projects have performed model verification and performance evaluation, systematic analysis of the types and complexity of variables used in the parameterization of the snow physics process remains insufficient. Menard et al. (2021) gave a summarized comparison of snow-related characteristics and their references briefly. However, they did not present a thorough representation of snow-related parameterization for twenty-seven models from 22 modeling teams. Since each model's documentation in ESM-SnowMIP is not perfect or even not provided, we decided to review the following LSMs that have comprehensive and informative documentation for analyzing the snow-related parameterization: 1) the Community Land Model version 5 (CLM 5; Lawrence et al., 2018) – the land model for the Community Earth System Model (CESM; Danabasoglu et al., 2020); 2) the Hydrology Tiled ECMWF Scheme of Surface Exchanges over Land (HTESSEL; Dutra et al., 2009) – the operational land model for the European Centre for Medium-Range Weather Forecasts (ECMWF); 3) the Canadian Land Surface Scheme (CLASS; Verseghy, 2012) – the land surface schemes in the Canadian Earth system model (CanESM; Swart et al., 2019) developed by the Environment and Climate Change Canada (ECCC); 4) the Joint UK Land Environment Simulator (JULES; Best et al., 2011) – the land surface schemes in both the physical climate model HadGEM3-GC3 (Menary et al., 2018) and the United Kingdom's Earth System Model (UKESM; Sellar et al., 2019); and 5) the Interaction Soil-Biosphere-Atmosphere (ISBA; Decharme et al., 2016), which constitutes the 'nature' tile of the platform SURFEX (SURFace EXternalisée; Masson et al., 2013) as the externalized land surface scheme in the Centre National de Recherches Météorologique Coupled global climate Model (CNRM-CM; Voldoire et al., 2012). Additionally, we examined the LSMs that are not included in the ESM-SnowMIP: 1) the Unified Noah Land Surface Model (Noah LSM; Koren et al., 1999) – the operational land surface model of the National Centers for Environmental Prediction (NCEP); 2) the Community Noah Land Surface Model with Multi-

https://doi.org/10.5194/tc-2021-319
Preprint. Discussion started: 30 November 2021

Parameterization Options (Noah-MP; Niu et al., 2011); and 3) the Biosphere-Atmosphere Transfer Scheme (BATS; Dickinson et al., 1993). The Noah LSM and Noah-MP are the current and future generations of Korean Integrated Model (KIM; Hong et al., 2018) operational forecasting systems of the Republic of Korea, respectively. We need to select representative models to derive ideas for future model improvement and concretely compare and analyze for the parameterization of the snow physics process. we analyzed BATS model because albedo parameterization of the Common Land Model (CoLM; Li et al., 2017), JSBACH (Reick et al., 2021), and JSBACH3-PF (Ekici et al., 2014) as well as Noah-MP is adapted from BATS method (Dickinson et al., 1986).

Therefore, this study attempts to understand the variables and parameters considered in each land surface model's current situation by looking at the parameters of three significant snow-related variables—snow cover, snow albedo, and snow density—through eight LSMs: Noah LSM, HTESSEL, BATS, CLASS, Noah-MP, CLM 5, JULES, and ISBA. In addition, we intend to provide insights into variables that may be considered in different models through a comparison of parameterization methods. Sections 2, 3, and 4 compare and analyze eight LSMs in relation to the parameterization of snow cover, snow albedo, and snow density, respectively. We focused on the new snow density in the snow density part because snow compaction due to destructive metamorphism or overburden, melting, and drifting snow is too complicated. Section 5 provides insights for LSM improvement by discussing the comparison results and significant variables in other previous studies and presents summaries in Section 6.

2 Snow cover parameterization in LSMs

Model studies show that snow cover changes significantly influence the land surface energy balance and ground temperature (Thomas and Rowntree, 1992; Viterbo and Betts, 1999). Since the snow-covered ground albedo is much higher than the snow-free ground albedo, accurate prediction of the presence or absence of snow is crucial for understanding near-surface energy balance. Snow cover can change grassland albedo by approximately 3–4 and mountain albedo by 2–3 (Thomas and Rowntree, 1992; Betts and Ball, 1997; Jin et al., 2002; Barlage et al., 2010). Armstrong and Brun (2008) presented snow depth, snow density, and SWE as fundamental properties when describing snow cover.

Table 1 expressed the variables considered in the eight LSMs, including the main variables such as snow depth, snow density, roughness length and SWE. All LSMs except BATS, JULES, ISBA used the SWE to parameterize snow cover. The snow cover parameterization of Noah LSM and CLM 5 considered the threshold of SWE. The Noah LSM's snow cover formula reflects the land surface type through the SWE threshold parameter. CLM 5 also considers the land surface type when using the SWE threshold, and it especially takes into account sub-grid geomorphic variation, the main difference among LSMs. HTESSEL is the simplest of the eight LSMs and considers only the SWE and snow density. The CLASS model used the snow depth and the snow depth threshold instead of the SWE and the SWE threshold, and the snow depth is calculated from SWE and snow density. The BATS, JULES, ISBA and Noah-MP model are different from the others in that it utilizes snow depth and roughness length to parameterize snow cover. Besides, they used different values of roughness length according to the land surface type.

https://doi.org/10.5194/tc-2021-319
Preprint. Discussion started: 30 November 2021

Table 2 presents the different formulations for snow cover fraction in the eight LSMs. The SWE, the SWE threshold value ($W_{\max}$) when the snow cover is 1, and the distribution shape parameter (P_s) determine the snow cover parameterization of the Noah LSM (Eq. (a) in Table 2) (Koren et al., 1999). If the SWE exceeds $W_{\max}$, the snow cover is assumed to be 1. Anderson (1973) considered the range of P_s as a value between 2 and 4 in the empirical equation for snow cover fraction, and the Noah LSM applied a fixed value of 2.6. The primary empirical values—the $W_{\max}$ and the P_s—affect the land surface albedo because the snow cover fraction variation controls the snow albedo. The Noah LSM provides $W_{\max}$ values according to the land surface types based on the modified International Geosphere-Biosphere Program (IGBP) MODIS Noah classification. The Noah LSM designate $W_{\max}$ values as 0.08 m, 0.04 m, 0.025 m, 0.02 m, and 0.01m for forests, short vegetation, tundra, low vegetation areas such as snow, glacial areas, and water bodies, respectively. Wang and Zeng (2010) showed that the $W_{\max}$ value for grassland and forest tend to have similar simulation results to the observed values when adjusted to 0.01 m and 0.2 m instead of 0.04 m and 0.08 m for each vegetation type. Livneh et al. (2010) improved the $W_{\max}$ value to 0.02 m for non-forest and 0.04 m for the forest, reflecting the study area's vegetation properties. Therefore, we need to find an appropriate $W_{\max}$ value that can guide the snow cover fraction following its observation value depending on the land surface type.

HTESSEL parameterized the snow cover fraction using a formulation of SWE and low and high densities of snow, which showed a different route for the snow cover parameterization. The existing HTESSEL snow cover was calculated only as an SWE function (Eq. (b)). However, the new scheme introduced snow density in addition to the SWE (Eq. (c)). The existing parameterization method was expressed as extreme values of both snow densities, while the modified parameterization method was improved to reflect the changing snow density. The new scheme is straightforward, but it reflects the variability of snow cover between the beginning of a cold season (low snow density) and the end of an ablation season (high snow density) (Dutra et al., 2009). At the beginning of the cold season, it is easy to cover the entire grid even if there is a small SWE. On the other hand, since snow melting that creates non-snow patches at the snow depletion period, more SWE is required for snow cover to be 1 in one grid. HTESSEL introduced snow density to the simulation of seasonal snow cover variation, thus devising a snow cover parameterization scheme that could reflect the physical process of snow.

In BATS, the snow cover fraction is measured in terms of the snow depth, so it changes over time by subtracting the sublimation rate and snow melting from the snowfall rate. BATS parameterized the snow cover fraction, divided into areas with and without vegetation (Dickinson et al., 1993). For land surfaces without vegetation, it was parameterized with 0.1 m and snow depth (Eq. (d)), while for land surface with vegetation, it was parameterized as a function of the snow depth and the roughness length multiplied by 10 (Eq. (e)). Yang et al. (1997) described the total fraction of the grid square covered by snow (f_s) as

$$f_s = f_{s,g}(1-\sigma_f) + f_{s,v}\sigma_f, \tag{1}$$

where σ_f is green vegetation fraction, $f_{s,g}$ and $f_{s,v}$ are fraction of ground covered by snow and fraction of vegetation covered by snow, respectively. Eq. (d) from Table 2 clarified as

$$f_{s,g} = D_{sn}/(10z_{0g} + D_{sn}), \tag{2}$$

https://doi.org/10.5194/tc-2021-319
Preprint. Discussion started: 30 November 2021

where D_{sn} is snow depth and z_{0g} is roughness length for bare soil and the value is designated as 0.01 m (Yang et al., 1997). The formation of equation (2) is same as Eq. (e) in Table 2.

Yang et al. (1997) upgraded the snow cover fraction scheme using different roughness lengths according to the land surface type and snow depth (Eq. (f)). This new scheme reflects the aspect from Jordan et al. (2008) that snow cover and albedo are related to the vegetation and roughness length. Yang et al. (1997) showed that the simulated snow cover fraction and surface albedo has a close agreement with the observed, especially in short vegetation. Figure 1 demonstrates the comparison of BATS formulation (Eqs. (d), (e), (f)) for snow cover fraction in the case of short grass land cover. Eq. (f) may be appropriate for grasses and agricultural lands (Yang et al., 1997) because it illustrates that the higher the snow depth, the faster cover the short grass. BATS focused on the snow-ground process and did not distinguish between the soil temperature and the lowest layer of snow. Geothermal heat can reach the upper surface of the snow by conduction. Nevertheless, it was assumed to ignore snow melting at the bottom of the snowpack (Dickinson et al., 1993).

CLASS parameterized the snow cover fraction using the snow depth (D_{sn}) and the threshold value of snow depth ($D_{sn,lim}$) (Eq. (g)) (Verseghy, 2012). The threshold of the snow depth ($D_{sn,lim}$) applied to 0.1 m. If the snow depth (D_{sn}) is >0.1 m, the snow cover is considered 1. When the snow depth is <0.1 m, parameterization for snow cover fraction uses Eq. (g) in Table 2. At this time, CLASS calculates the snow depth by dividing the SWE by the snow density (Eq. (h)). Melton et al. (2019) recently suggested another parameterization for snow cover with the exponential form (Eq. (i)) proposed by Brown et al. (2003). In CLASS, the snow depth threshold was assumed to be the same value regardless of the land surface type, so there could be a limitation in that it cannot follow the variability of the snow cover fraction according to the land cover type.

Noah-MP parameterizes the snow cover fraction using roughness length, snow depth as well as snow density. Yang et al. (1997) proposed the Hyperbolic Tangent(tanh) formulation (Eq. (f)) because they need to reflect two stages of snow depth and snow albedo relationship: sharply increasing albedo stage and slowly increasing albedo stage per changing snow depth. This formulation has a limitation of too fast covering snow, so Eq. (f) does not consider the seasonal variation of snow cover patterns. Niu and Yang (2007) perceived this limitation of Eq. (f) which is fit for shorter vegetation, and revised formulation Eq. (j) using a melting factor for snow cover fraction (F_{melt}). F_{melt} (Eq. (k)) calculates using fresh snow density, 100 kg m^{-3}, and current snow density (Eq. (l)) with determining melting curves parameter M which can be adjustable.

CLM 5 parameterizes the accumulation and depletion of snow cover fraction separately (Lawrence et al., 2018). The parameterization of the snow cover fraction during the snow accumulation phase (Eq. (m)) reflects the new snow amount ($q_{snow}\Delta t$), a constant (k_{accum}) whose default value is 0.1, and the snow cover fraction (f_s^n) from the previous time step. The snow cover fraction parameterization during the snow ablation phase (Eq. (n)) shows similarity with Noah LSM in that SWE and SWE thresholds influence the depletion curve. Swenson and Lawrence (2012) developed the empirically derived expression Eqs. (m) and (n). Significantly, CLM 5 newly incorporates a parameter N_{melt} that changes depending on the geomorphic variability within the grid cell as shown in Eq. (o) in Table 2 (Swenson and Lawrence, 2012; Lawrence et al., 2018). N_{melt} controls the shape of the snow-covered area (Figure 2). If N_{melt} values are low, the topographic variability of regions are high. CLM 5 calculates N_{melt} from the standard deviation of the 1 km-resolution DEM elevation within a grid cell. However, in the glacier region, N_{melt} implemented a direct value of 10 because the terrain there could be very flat. This new parameterization scheme

https://doi.org/10.5194/tc-2021-319
Preprint. Discussion started: 30 November 2021

roughly demonstrates the results of Jordan et al. (2008) in that the topographic variation of the ground causes changes in the snow cover depth.

Snow cover fraction parameterization in JULES (Eq. (p)) is identical with BATS snow cover fraction for vegetation (Eq. (e)). JULES adopted only snow cover fraction using snow density and roughness length for bare soil (Best et al., 2011) and ignored the vegetation fraction for calculating the snow cover fraction. ISBA separates snow cover fraction parameterization for bare soil (Eq. (q)) and vegetation (Eq. (r)) similarly to BATS (Table 2). ISBA formulation of snow cover fraction for bare soil is similar to CLASS using snow depth and snow depth thresholds. Besides, the ISBA formulation structure of snow cover fraction for vegetation is the same as BATS; the coefficient is different between ISBA and BATS as 2 and 10, respectively. The vegetation roughness length in ISBA designated as specific value depending on each vegetation type(Decharme et al., 2019). In particular, ISBA used equation (1) with GVF for the average between the snow cover fraction in the vegetated ($f_{s,v}$) and non-vegetated ($f_{s,g}$) as a part of a grid cell concept similar to BATS (Decharme et al., 2016). Among the eight LSMs, only BATS and ISBA consider GVF directly for snow cover parameterization, and BATS, Noah-MP, JULES, and ISBA account for roughness length.

3 Snow albedo parameterization in LSMs

Snow albedo is the rate of reflection of incident radiation on snowpack, which plays an essential role in the energy balance of the land surface over snow during the melting season (Warren and Wiscombe, 1980; Wiscombe and Warren, 1980). One of the land surface model's main objectives is the accurate distribution of incident radiation into radiation, sensible heat, and latent heat fluxes. Net radiation is a concept that includes both upward & downward shortwave radiation and upward & downward longwave radiation in the surface energy balance. The surface albedo—the ratio of reflected solar radiation to the incident solar radiation—determines the energy transfer between the air and land surface. Typical albedo values are as high as 80–90 % on a non-melting snow surface (Armstrong and Brun, 2008) and are expressed as various values according to the state of snow surface (fresh, dry snow; old, dry snow; wet snow; melting ice/snow) or the land surface type (snow-covered forest, snow-free vegetation/soil, water) (Table 3).

One of the most rapid changes in land surface albedo is the presence or absence of snow cover. Noah LSM, CLM 5, and JULES use the snow cover fraction as a significant variable in the albedo parameterization (Table 4). Thus, they calculate snow albedo by summing the snow-free albedo and snow-covered albedo according to the snow cover ratio. In Jordan et al. (2008), the interception of radiation by vegetation strongly changes the albedo in the snow-covered area. The vegetation type, vegetation density, snow accumulation on the canopy, and incident radiation can affect snow albedo alteration (Jordan et al., 2008). For instance, Noah LSM, HTESSEL, BATS, and CLM 5 consider the vegetation effects on snow albedo parameterization indirectly by using the maximum snow albedo for each vegetation type or applying the green vegetation fraction value. The albedo for each grid point can be calculated by linearly weighting the snow-free albedo and snow and vegetation albedo in the snow-covered area. In particular, BATS, CLM 5, and JULES were relatively complex land surface models because they

https://doi.org/10.5194/tc-2021-319
Preprint. Discussion started: 30 November 2021


The Cryosphere Discussions

identify direct & diffuse albedo, visible & near-infrared albedo separately, taking into account all the effects of the solar zenith angle, and ice grain size. Additionally, BATS and CLM 5 considers dust and carbon.

Table 5 presents snow albedo parameterization in eight different LSMs. In the Noah LSM, the albedo is parameterized by a weighted average of the snow-free albedo and the snow-covered albedo (Eq. (a) in Table 5). The snow albedo is closely related to the snow cover fraction (Brun et al., 2008). The snow-covered patch can be distributed differently due to the slope or altitude, the spatial direction of a snowdrift, and the snow melting period. Moreover, the snow albedo on the surface can increase noticeably as the vegetation rate decreases. When there is short or large vegetation, the snow-covered area may exist in the form of a patch. The surface albedo is parameterized to account for this vegetation effect, as shown in Eq. (b), using the green vegetation fraction (σ_f) value.

Noah LSM treated the maximum new snow albedo parameterization for fresh snow by calculating the satellite-based snow albedo ($\alpha_{\max,sat}$), the maximum snow albedo coefficient ($\alpha_{\max,CofE}$), and the proportionality coefficient (C) as shown in Eq. (c). The proportionality coefficient is fixed at 0.5, but Livneh et al. (2010) adjusted it to 1. The maximum snow albedo coefficient, 0.85, determines the maximum albedo value of newly fallen snow. The new maximum snow albedo equal to 0.85 in Noah LSM was the same value used in the Distributed Hydrology Soil Vegetation Model (DHSVM; Wigmosta et al., 1994) and Variable Infiltration Capacity Macroscale Hydrologic Model (VIC; Andreadis et al., 2009). SnowModel default (Liston and Elder, 2006), CLASS model (Verseghy, 1991) was set to 0.8, while SnowModel (Sproles et al., 2013) used the maximum albedo value after new snowfall as 0.8 in unforested and 0.6 in forested areas. According to the snow melting condition, the new maximum snow albedo used in the SNOWPACK (Bartelt and Lehning, 2002) was 0.95 in the non-melt condition and 0.7 in the melt condition. In the case of BATS (Dickinson et al., 1993), it was set to 0.85/0.65 (visible/near-infrared area) in the non-melt condition and 0.75/0.15 in the melt condition.

Livneh et al. (2010) adapted the albedo-decay parameterization proposed by Wigmosta et al. (1994) for the DHSVM. The albedo-decay scheme can change the coefficient over time depending on whether the snow is accumulated (slow decay) or ablated (fast decay) (Eq. (d)). The albedo decay scheme in Noah LSM reflects the snow accumulation season as a default setting. At the snow accumulation, the snow temperature is < 273.16 K, and A and B are set to 0.94 and 0.58 in Eq. (d), respectively. When the snow decays, the snow temperature is ≥ 273.16 K, A and B are set to 0.82 and 0.46 in Eq. (d), respectively. Storck (2000) calculated A's values in the albedo-decay scheme as 0.92 and 0.7 for the accumulation and ablation seasons, respectively, based on observations of the shelterwood site. Sun et al. (2019) showed that the A value at the time of snow accumulation could be in the possible range 0.87–0.99 in the same formula (Eq. (d)) as the Noah LSM. They derived 0.9–0.96 as the optimal value ranges for snow accumulation phase for different areas. While the possible range for the A value at the time of snowfall ablation season was set to 0.82–0.91, the optimal value was almost the same range at 0.83–0.91 (Sun et al., 2019). In addition, Malik et al. (2014) suggested improved values only for the time of snow accumulation, and A was in the range 0.9–0.94, and B was in the range 0.5–0.66 for different areas.

The original scheme of the snow albedo for HTESSEL follows the formulation of Baker et al. (1990), Verseghy (1991), Douville et al. (1995) and separates into melting and non-melting cases. Its formulation structure is the same as the past version of ISBA parameterization (Mölders et al., 2007). If the snow does not melt, the albedo uses a linearly decaying coefficient

https://doi.org/10.5194/tc-2021-319
Preprint. Discussion started: 30 November 2021


The Cryosphere Discussions
Open Access
EGU

($\gamma_a = 0.008$). When the snow melting exceeds 0 or when the snow surface temperature is > 2 K lower than the freezing point temperature, HTESSEL parameterized the albedo as Eq. (e) in Table 5 with the exponential decay factor ($\gamma_f = 0.24$) and the minimum albedo ($\alpha_{\min,H} = 0.5$). In other words, the higher the temperature, the more quickly the snow albedo decreases. When the amount of new snowfall exceeds 1 kg m^{-2} hr^{-1}, the maximum snow albedo is set to 0.85. However, Pedersen and Winther (2005) and Mölders et al. (2007) pointed out that the original scheme has a disadvantage of too low threshold value when used for numerical forecasting in snow albedo parameterization. The parameterization was improved as shown in Eq. (f), so the snow albedo was continuously reset. HTESSEL assumed that 10 kg m^{-2} of new snowfall is required to reset the maximum snow albedo to 0.85 consistently.

The original scheme uses a fixed value of 0.15 for albedo under a canopy regarding the vegetation's influence. However, this is insufficient to describe the variability of snow albedos according to the vegetation characteristics. As a result of observations in a forest area with snow intercepted by vegetation, the albedo appeared to be 0.3 immediately after heavy snowfall and changed to 0.2 after a few days according to the forest type (Betts and Ball, 1997; Viterbo and Betts, 1999). The snow intercepted by vegetation disappears due to wind blowing in cold temperatures or snow melting in warm temperatures. Therefore, HTESSEL set the albedo for each vegetation condition differently according to the 16 types of IGBP vegetation. HTESSEL used the white-sky albedo climate values (2000–2004) in the 0.3–5 μm band of the northern hemisphere with snow on the ground suggested by Moody et al. (2007).

BATS calculates the snow albedo by classifying the diffuse and direct radiation and parameterizes each albedo by separating it into visible and near-infrared regions. Concerning the diffuse radiation, when the solar zenith angle is less than 60°, the new snow albedo for visible radiation incident is 0.95, and the new snow albedo for near-infrared solar radiation is 0.65. The albedo decay parameterization method applies over time (Dickinson et al., 1993) (Eqs. (g) and (h) in Table 5). As a factor associated with snow decay, BATS calculates the decreasing term F_{age} through equations (3)–(11) (Wang et al., 2020): F_{age} give the fractional reduction of snow albedo due to growth of snow grain size and accumulation of dirt and soot by

$$F_{age} = \frac{tauss^t}{(tauss^t + 1)}, \tag{3}$$

where $tauss^t$ is a nondimensional age of snow, defined as

$$tauss^t = \begin{cases} 0, & \text{for } swe^t = 0 \text{ or } swe^t > 800; \\ \max(0, sge^t), & \text{for others,} \end{cases} \tag{4}$$

with swe^t representing the snow water equivalents of the current time step. The nondimensional age of snow sge^t depends on a model prognostic variable δ_a as follows

$$sge^t = \left(tauss^{t-1} + \delta_a\right) \times (1 - \delta_s), \tag{5}$$

where δ_s is expressed as

$$\delta_s = \frac{\max(0, swe^t - swe^{t-1})}{swe_c}. \tag{6}$$

https://doi.org/10.5194/tc-2021-319
Preprint. Discussion started: 30 November 2021


The Cryosphere Discussions

Here, $swe^t - swe^{t-1}$ is the change of snow water equivalent (in mm or kg m^{-2}) in one time step Δt, and swe_c indicates the critical value of new snow water equivalent to fully cover the old snow, assumed to be 1 mm; and δ_a is parameterized as

$$\delta_a = 10^{-6} \times \Delta t \times (Age_1 + Age_2 + Age_3)\,. \tag{7}$$

In (7), Age_1 represents the effect of growing snow particle size by vapor diffusion which is formulated as

$$Age_1 = \exp(arg) \tag{8}$$

where

$$arg = 5000\left(\frac{1}{T_f} - \frac{1}{T_g}\right), \tag{9}$$

with T_f the freezing temperature (273.16 K) and T_g the ground temperature (K); Age_2 reflects the effect of recrystallization of melting moisture or close to it and is represented as

$$Age_2 = \min[1, \exp(10 \times arg)]; \tag{10}$$

and Age_3 represents the effects of dust and soot as follows:

$$Age_3 = \begin{cases} 0.01 & \text{over Antarctica;} \\ 0.3 & \text{elsewhere.} \end{cases} \tag{11}$$

BATS designated Age_3 as 0.01 for Antarctica and 0.3 for other areas (Dickinson et al., 1993).

Concerning the direct radiation, BATS parameterizes the new snow albedo using factors such as the diffuse snow albedo and the solar zenith angle (Eqs. (i) and (j) in Table 5). F_{zenith} is a factor to account for solar zenith angle impact, calculated as

$$F_{zenith} = \frac{1}{b}\left\{\frac{b+1}{[1+2b\cos(zen)]} - 1\right\}, F_{zenith} = 0 \text{ if } \cos(zen) > 0.5, \tag{12}$$

where b can be adjustable to best available data, and it is designated $b = 2.0$ in BATS (Dickinson et al., 1993). Equation (12) has the property for all b that it vanishes at $cos(zen) = 0.5$, so F_{zenith} values equal to 0. The value of b is unity at $cos(zen) = 0$ which is the same as the solar zenith angle in the horizontal plane, so F_{zenith} is equal to 1. In Wang et al. (2020), the method of parameterizing F_{zenith} was further simplified as follows:

$$F_{zenith} = \max\left\{\frac{1.5}{[1+\cos(zen)]} - 0.5, 0\right\}, \tag{13}$$

where F_{zenith} is a value between 0 and 1; for example, when the solar zenith angle exceeds 60 degrees, the snow albedo for visibility area increases.

https://doi.org/10.5194/tc-2021-319
Preprint. Discussion started: 30 November 2021

315 CLASS assumes a single snow albedo for direct and diffusive radiation. If the snow depth is over 1 cm, the new snow albedo is supposed to be 0.84 in the original CLASS. CLASS calculated the new snow albedo as the weighted average of 0.84 and the ground albedo before snowfall. Fresh snowfall albedo in CLASS (Eq. (k)) has the same structure as HTESSEL's new snowfall albedo parameterization (Eq. (f)). However, there is a difference in that CLASS assigned a value of 1 mm for the SWE threshold of 100% snow cover. In addition, CLASS assumed that the snow albedo in the current time step is over 0.55
320 (Eq. (l)).

Recently, Melton et al. (2020) described the Canadian Land Surface Scheme including Biogeochemical Cycles (CLASSIC; v.1.0) as the coupled model framework of the CLASS (Verseghy, 2017) and the Canadian Terrestrial Ecosystem Model (CTEM; Melton and Arora, 2016). CLASSIC model parameterized snow albedo decay based on the data of Aguado (1985), Robinson and Kukla (1984), and Dirmhirn and Eaton (1975). Melton et al. (2019) showed that it is the same as empirical exponential
325 decay functions applied to CLASS-CTEM by Verseghy (2017). The background old snow value was 0.55 in the original CLASS (Eq. (l)). However, the background old snow value ($\alpha_{sn,total,old}$) applied as 0.5 if the snow melting ratio was >0 (melting snow condition) unless it applied as 0.7 in the case of dry snow in the updated CLASS in CLASSIC (Eq. (m)). The CLASSIC classified three categories: total albedo, visible albedo, and near-infrared albedo that have typical values for fresh snow, old dry snow, and melting snow as shown in Table 6 (Aguado, 1985; Robinson and Kukla, 1984; Dirmhirn and Eaton,
330 1975). CLASSIC calculated the albedos of visible and near-infrared as Eqs. (n) and (o) for dry snow and Eqs. (p) and (q) for melting snow, respectively.

Noah-MP implemented two options for parameterizing snow albedo from BATS and CLASS schemes. The BATS scheme of snow albedo accounts for fresh snow albedo, variation in snow age, solar zenith angle, snow grain size growth, and dirt or soot on snow (Niu et al., 2011). The CLASS scheme of snow albedo considers fresh snow albedo and snow age (Niu et al.,
335 2011). Noah-MP uses an old version of the CLASS scheme as Eqs. (k) and (l), so it does not distinguish the wet and dry snow conditions as well as snow albedo of the visible and near-infrared area. Niu et al. (2011) describes that the CLASS scheme tend to decrease snow surface albedo easily compared to the BATS scheme due to the strong aging factor.

CLM 5 calculates the ground albedo by a weighted average of the overall direct beam albedo and diffuse albedo. The albedo value in CLM 5 adapted MODIS MCD43B3 v5 data for 2001–2015 (Lawrence et al., 2019). It parameterizes the direct and
340 diffuse albedos using the fraction of the ground covered with snow as in Eqs. (r) and (s) in Table 5, respectively (Lawrence et al., 2018). In addition, the direct beam albedo and diffuse albedo are various according to the land surface type. The representative types are glaciers, unfrozen lakes, frozen lakes, and soil surfaces. Glacier albedos have a prescribed value depending on the range of visible and near-infrared (Cuffey, 2010), so the visible albedo is 0.6 and near-infrared albedo is 0.4 regardless of direct or diffuse albedo (Eqs. (t) and (u) in Table 5). Frozen lake albedos have the same fixed value as glacier albedo (Bonan,
345 1996), direct and diffusive albedos of an unfrozen lake are parameterized following the cosine of the solar zenith angle (Eq. (v)) (Lawrence et al., 2018).

Soil albedo depends on the soil color and varies with the moisture content of the first soil layer (Bonan, 1996). Soil albedo is calculated differently according to the change in soil moisture content ($\Delta = 0.11 - 0.40\theta_1 > 0$) based on the saturated albedo and dry albedo determined according to the soil color (Eq. (w)). The soil color of the CLM 5 is pre-specified for the CLM

https://doi.org/10.5194/tc-2021-319
Preprint. Discussion started: 30 November 2021

grid using the method of Lawrence and Chase (2007). The soil color is adjusted to one of 20 averaging the fitted monthly soil colors over all snow-free months and compared with the MODIS monthly local solar noon all-sky surface albedo described in Strahler et al. (1999) and Schaaf et al. (2002).

CLM 5 simulates the snow albedo and solar absorption within the snow layer with the Snow, Ice, and Aerosol Radiative Model (SNICAR), which was implemented in CLM version 3 (Flanner, 2005; Flanner et al., 2007). SNICAR includes the two-stream radiative transfer solution of Toon et al. (1989) and uses the theory of Wiscombe and Warren (1980). The albedo and the vertical absorption profile depend on the solar zenith angle, the albedo of the surface under the snow, the mass concentration of atmospheric-deposited aerosols (black carbon, mineral dust, and organic carbon), and the ice effective grain size (Lawrence et al., 2018).

JULES has two types of scheme: the diagnostic albedo scheme and the prognostic albedo scheme. The diagnostic albedo calculates snow albedo as Eq. (x1) in Table 5 using surface temperature (T_g), snow aging parameter (k_1), snow albedo threshold temperature (T_c), and cold deep snow albedo depending on the vegetation type (α_{cds}) (Best et al., 2011). JULES derives the weighted average of surface albedo as Eq. (x2) considering snow depth (D_{sn}) and surface masking snow depth (D_m). The prognostic albedo in JULES calculates total surface albedo by using snow cover fraction, snow albedo, and snow-free albedo like Eq. (a) of Noah LSM. The prognostic albedo scheme calculates both diffuse visible and near-infrared areas as Eqs. (y1) and (y2), respectively (Best et al., 2011). The diffuse scheme includes timely changing grain size (r) and fresh snow grain size (r_0). For the direct radiation albedo, r in Eqs. (y1) and (y2) need to be replaced by effective grain size (r_e) as

$$r_e = [1 + 0.77(\mu - 0.65)]^2 r, \tag{14}$$

calculated using the cosine of the zenith angle (μ) and grain size (r). The current state of grain size is calculated every time step with snowfall rate S_f by

$$r(t+\delta t) = [r(t)^2 + \frac{G_r}{\pi}\delta t]^{1/2} - [r(t) - r_0]\frac{S_f \delta t}{d_0}, \tag{15}$$

where d_0 is fresh snow depth and r_0 is 50μm for fresh snow (2.5 kg m^{-2} fresh snow mass required to refresh the albedo) and G_r is the empirical growth rate of snow grain area expressed as

$$G_r = \begin{cases} 0.6 & T_g = T_m \text{ (melting snow);} \\ 0.06 & T_g < T_m,\ r < 150\mu\text{m (cold fresh snow);} \\ A_s \exp(-4550/T_g) & T_g < T_m,\ r > 150\mu\text{m (cold aged snow).} \end{cases} \tag{16}$$

In Equation (16), A_s is set to $0.23 * 10^6 \mu$ m^2 S^{-1}. The prognostic albedo scheme in JULES consider direct and diffuse albedo from visible and near-infrared area same as BATS and CLM5. This scheme incorporates ice grain size affected by surface temperature and snowfall rate as the significant factor to calculate snow albedo.

ISBA calculates snow albedo from 3 distinct bands (Eqs. (z1), (z3), and (z5) in Table 5), the first band with the ultraviolet and visible range (0.3–0.8 μm), the second and the third band with near-infrared ranges (0.8–1.5 and 1.5–2.8 μm) following Brun

https://doi.org/10.5194/tc-2021-319
Preprint. Discussion started: 30 November 2021

et al. (1992). For the first snow layer, snow albedo account for snow optical diameter, the near surface atmospheric pressure, and the age of the first snow layer in days (Eq. (z1)). Only first snow layer considers atmospheric pressure and time of snow albedo decay ratio by impurities. The albedo scheme for the second and the third snow layer take into account snow grain size. The optical diameter of snow ($d_{\mathrm{opt}}(i)$) is parameterized as

$$d_{\mathrm{opt}}(i) = \min[d_{max}, g_1 + g_2 \times \rho_{\mathrm{s}}(i)^4 + g_3 \times \min(15, A_{sn}(i))] \tag{17}$$

where d_{max} is the maximum snow diameter value, and g_1 (1.6×10^{-4} m), g_2 (1.1×10^{-13} m^{13} kg^{-4}) are coefficients calculated from Anderson et al. (1976). g_3 (0.5×10^{-4} m day^{-1}) is the increase rate of the optical diameter of snow with snow age in Equation (17). β_{sn} is the extinction coefficient of snow affected by snow density and optical diameter of snow (Eqs. (z2), (z4), and (z6) in Table 5). Bohren and Barkstrom (1974) used a constant 3.8×10^{-3} m$^{5/2}$ kg^{-1} for the snow extinction coefficient, but it changed to 0.00192 and 0.01098 for the first and the second snow layers (Eqs. (z2) and (z4)).

4 Snow density parameterization in LSMs

Snowfall amounts are measured with the snow depth and SWE when the snow melts. Typical snow rates are 1 cm h^{-1} or 0.8 mm h^{-1}. The LSMs normally calculate snow depth by dividing the SWE by the snow density. The density of newly fallen snow is approximately 20–300 kg m^{-3}, and the dry snow density is about 60–120 kg m^{-3} with the condition of low-to-moderate winds, while it increases with the condition of wet snow, sleet, and wind-packed snow. When precipitation mixes snow and rain, the new snow density exceeds 300 kg m^{-3}. When snow falls by strong winds, the snow particles become fragmented and small-grained. As the wind speed of 1 m s^{-1} increases, the density gradually increases to 20 kg m^{-3} (Jordan et al., 1999). Therefore, snow characteristics (dry/wet) and wind conditions in addition to temperature affect the new snow density.

The LSMs considered different variables for calculating the snow density and snow depth (Table 7). Noah LSM, HTESSEL, CLM5, ISBA, and Noah-MP used air temperature to calculate the new snow density. Among these LSMs, HTESSEL, CLM 5, and ISBA had in common that they considered both the temperature and wind effects when calculating the new snow density. Jordan et al. (2008) also recognized the effect of wind speed, and the variation of wind speed caused by air pressure affects the snow depth on the slope, leading to snow erosion on the slope's upwind side and snow deposition on its lee side. BATS includes complex snow physics such as SWE, snow grain size, and the effects of dust and soot for calculating snow density changes. CLASS parameterizes the snow density updated over time with the maximum snow density calculated by the snow depth and the empirical constant according to the snow temperature. The time tendency of snow density in ISBA is affected by the snow density, vertical stress, snow viscosity, and wind-driven compaction rate in each layer. The snow density over a timestep in JULES is updated by compactive viscosity, ice and liquid water contents for the mass of snow above the layer, snow density, and the temperature of the k-th snow layer.

The LSMs parameterize the new snow density differently to estimate the snow depth as in Table 8. The new snow depth in Noah LSM is calculated by dividing the new SWE by the new snow density (Eq. (a)). If the sum of the existing and the new snow depth is $< 1.0E^{-3}$, the LSM took the higher value of the snow density between the new and the existing snow density.

https://doi.org/10.5194/tc-2021-319
Preprint. Discussion started: 30 November 2021


The Cryosphere Discussions

If the sum of the existing and the new snow depth is $\geq 1.0E^{-3}$, the snow density is parameterized by dividing the existing and new SWE by the sum of the existing and the new snow depth. Noah LSM uses the equation of Gottlib (1980) for calculating the new snow density (Koren et al., 1999). The density of new snow is a function of 2 m temperature above the ground when the 2 m temperature exceeds -15 °C. The density of fresh snow is 0.05 g cm^3 when the 2 m air temperature is $\leq -15\,^{\circ}\mathrm{C}$ (Eq. (b) in Table 8). According to the parameterization method, Figure 3 illustrates the relationship between temperature and new snow density. The minimum value of density of new snowfall is 0.05 g cm^3, and the density of new snowfall tends to increase as the temperature increases.

In HTESSEL, the snow depth value is inversely proportional to the snow density and snow cover fraction and is proportional to SWE (Dutra et al., 2009) (Eq. (c)). When calculating the snow depth, using the snow density and snow mass (similar to the SWE) is similar to those of Noah LSM, and the consideration of the snow cover fraction is similar to that in CLM 5. Eq. (d) shows the equation for obtaining the new snow density in HTESSEL. This equation is converted from a constant value to an equation using the equation of CROCUS (Brun et al., 1989, 1992) and is a parameterization method that expresses the new snow density as a function of the temperature and wind speed (Dutra et al., 2009). In Eq. (d), a_{sn} is 109 kg m^{-3}, b_{sn} is 6 kg m^{-3}, and c_{sn} is 26 kg m$^{-7/2}s^{1/2}$. At this time, the snow density is limited to the range 50–450 kg m^{-3}.

The BATS model calculates the snow depth as shown in Eq. (e) in Table 8 by dividing the snow mass by the snow density (Dickinson et al., 1993; Yang et al., 1997). The snow density is parameterized as (Eq. (f)) with a snow aging factor according to the snow model and data of Anderson et al. (1976). The change of the snow aging factor is affected by the growth of snow particle size and accumulation of dust and soot (Dickinson et al., 1993; Yang et al., 1997). The snow aging factor explained in section 3 with Eq. (3) to (11).

CLASS also derives snow depth dividing SWE by snow density (Eq. (g) in Table 8). In the case of the maximum snow density, CLASS 2.7 used 300 kg m $^{-3}$ as a fixed value, whereas CLASS 3.6 parameterized as a function of the snow depth (Brown et al., 2006; Verseghy, 2012). If snow temperature below 0 °C, snow density decreases exponentially with time from the maximum mean density which is the calculated background snow density (Eq. (h)). The equation is derived from field measurements of Longley (1960) and Gold (1958) and express similarly to the albedo. Bartlett et al. (2006) found that the modified formula produced good results in the Boreal Ecosystem Research and Monitoring Sites (BERMS) (Old Aspen, Old Jack Pine, and Old Black Spruce). In the equation of the maximum snow density, the empirical constant (A_s) is 450 for cold snow case ($T_{snow} < 0\,^{\circ}\mathrm{C}$), and 700 for snow close to the melting point ($T_{snow} = 0\,^{\circ}\mathrm{C}$) according to Tabler et al. (1990) (Eq. (i)). This empirical constant is consistent with the results of Wakahama (1968) and Colbeck (1973), which both showed a tendency to increase the compression rate of snow density with wet snow (Brown et al., 2006).

Noah-MP calculates snow density or snow depth considering destructive metamorphism by temperature change, compaction by the weight of the overlying snow layers, and snow melting metamorphism according to Anderson et al. (1976). Noah-MP's snow layer determines by the total snow depth (Yang and Niu, 2003). If the snow depth is <0.045 m, snow layer does not exists. If the snow depth is ≥ 0.045 m, the first snow layer has a layer thickness as the total snow depth. When snow depth is ≥ 0.05 m, two layers produces, and when snow depth is ≥ 0.15 m, a third layer is created. The third snow layer is thick due to the compaction following Sun et al. (1999) (Niu et al., 2011). Snow depth is dividing snow on the ground by bulk density snowfall

https://doi.org/10.5194/tc-2021-319
Preprint. Discussion started: 30 November 2021


The Cryosphere Discussions

which is set to 120 when fresh snow density is smaller than 120 and parameterized as the following fresh snow density (Eqs. (j) and (k)). Fresh snow density in Noah-MP is calculated according to the Hedstrom and Pomeroy (1998) by Eq. (l) in Table 8. Fresh snow density mainly account for the surface air temperature and freezing temperature.

CLM 5 calculates the snow depth next time, adding new snow depth to the snow depth at the current time (Lawrence et al., 2018). CLM 5 parameterizes the new snow depth as the rate of change (Δz_{sno}, m), which is a function of the bulk density of newly fallen snow (ρ_{sn}, kg m^{-3}), the snow cover fraction (f_s), and the rate of solid precipitation reaching the ground ($q_{grnd,ice}$, kg m^{-2} s^{-1}) (Eq. (m)). In particular, CLM 5 considers the snow cover for estimating snow depth, like HTESSEL. The density of newly fallen snow parameterization incorporates summing the fresh snow density according to the temperature and wind (Eq. (n)). Eq. (o) shows the fresh snow density according to the temperature (ρ_T) in CLM 5 (Anderson et al., 1976; van Kampenhout et al., 2017), and the equation has a similar structure to that of the Noah LSM. However, CLM 5 has a difference in that it added the critical temperature, the freezing temperature of water (in K) + 2 K. Besides, the lowest air temperature parameterized in CLM 5 does not use a constant value like -0.05. CLM 5 utilized wind dependent term for the new snowfall density (ρ_w) as Eq. (p) from van Kampenhout et al. (2017) who considers both wind and temperature.

JULES have multi-layer snow model, snow density on k-th layer over a time step of length δt can be parameterized as Eq. (q) in Table 8. Snow density scheme in JULES account for the reference snow temperature ($k_s = 4000$ K), the snow melting point ($T_m = 273.15$ K), the temperature of the k-th snow layer (T_k, K), reference snow density ($\rho_0 = 50$ kg m^{-3}), snow density of the k-th snow layer (ρ_k, kg m^{-3}), and compactive viscosity ($\eta_0 = 10^7$ Pa s), and the mass of snow above the middle layer ($M_k = 0.5\,(I_k + W_k) + \sum_{i=1}^{k-1}(I_i + W_i)$), where I_k (kg m^{-2}) and W_k (kg m^{-2}) are an ice content and a liquid water content, respectively (Best et al., 2011). The layer thickness (d_k, m) which have the relationship with density and mass expressed by $\rho_k d_k = I_k + W_k$. This formulation is identical meaning with Noah LSM, BATS, CLASS, and Noah-MP.

The newly fallen snow density in ISBA is identical with fresh snow density scheme in HTESSEL (Eq. (d) in Table 8). ISBA expresses the time tendency of snow density as Eq. (r) like JULES, but the specific terms are different. The snow density changes by snow compaction due to vertical stress, the snow viscosity change (Brun et al., 1989), and wind-induced densification of snow layers (Brun et al., 1997). Especially, compaction rate of wind-driven snow densification parameterized as $\tau_{\mathrm{W}}(i)$ which describes precisely in Appendix B (Wind-induced densification of near-surface snow layers) from Decharme et al. (2016), and it is unique consideration of ISBA. The vertical stress in each layer can be parameterized as Eqs. (s) and (t) and vertical stress is also considered in JULES. It accounts for layer snow depth changes per time step (Δz), layer snow density (ρ_{sn}) and the acceleration of gravity (g) in every snow layer, but only the first snow layer used half mass of the uppermost layer as vertical stress effect. The snow viscosity in Eq. (u) is calculated by reference snow viscosity ($\eta_0 = 7622370$ Pa s), reference snow density ($\rho_0 = 250$ kg m-3), snow density in i-th layer ($\rho_{sn}(i)$), snow temperature in i-th layer ($T_{sn}(i)$), and the constants ($a_\eta = 0.1$ K^{-1}, $b_\eta = 0.023$ m^3 kg^{-1}, and $\Delta T_\eta = 5$ K). The decrease of viscosity with the presence of liquid water ($f_{\mathrm{W}}(i)$)is calculated by Eq. (v), where $W_{l\max}(i)$ (kg m^{-2}) and $W_l(i)$ (kg m^{-2}) refer to the maximum liquid-water-holding capacity and liquid water content in i-th layer.

https://doi.org/10.5194/tc-2021-319
Preprint. Discussion started: 30 November 2021

5 Future outlook

We visualized the current state of the art of snow cover fraction parameterization as Figure 4 by checking all significant variables of snow models in the supplementary table from Menard et al. (2021). Figure 4 shows that only a few LSMs used specific variables to discern the snow cover fraction, so snow model developers can easily compare differences among LSMs. The eight land surface models examined in this study calculate the snow cover fraction through "the threshold of the SWE and the SWE," for Noah LSM, and HTESSEL, "the critical value of the snow depth and snow depth," for CLASS. In addition, BATS, ISBA, JULES and Noah MP considers "the snow depth and roughness length" for deriving snow cover fraction (Figure 4). Noah MP additionally concerned snow density as the melting factor, and BATS and ISBA used the vegetation fraction separating the bare soil ground and vegetation covered ground for applying different roughness length according to the vegetation type and snow depth. Therefore, it is crucial to properly set the parameter values for "the threshold of snow depth or SWE" and the roughness length depending on the land surface type.

It is significant to derive an optimal parameter value that can reflect the local characteristics based on the same land type from the observation data. For instance, accurate snow cover estimation is crucial because snow cover fraction affects snow sublimation, soil heat flux, surface emissivity, and albedo in Noah LSM. That is why parameter improvements were attempted in Livneh et al. (2010) and Wang and Zeng (2010). The parameter values according to the land cover type provided in Noah LSM were set differently according to the height of the vegetation. The current version of the Noah LSM reflects the SWE for snow cover parameterization but does not consider the snow depth, snow density, roughness length, and green vegetation fraction. Therefore, considering snow depth (CLASS, RUC, ORCHIDEE-I, SPONSOR in Figure 4) or snow density (HTESSEL, EC-EARTH, Noah-MP, CoLM in Figure 4) for snow cover fraction parameterization could be better because these variables have timely varying characteristics due to the temperature. In addition, current state-of-the-art LSMs considers fixed roughness length value according to the vegetation cover (JULES, BATS, ISBA, and Noah MP). Therefore, a seasonal variation of roughness length needs to calculate snow cover fraction for reflecting vegetation effect.

Point-specific or 100% snow cover means that LSMs assume they do not express subgrid heterogeneity and inform ground conditions with or without snow (Figure 4). Since most LSMs have been developed for the atmospheric model, the representation of snow-covered and snow-free areas is significant for energy flux as the lower boundary condition. CABLE-SLI, CRHM, Crocus, ESCIMO, JSBACH, JSBACH3-PF, MATSIRO, SMAP, SNOWPACK, SWAP, VEG3D, SURFEX-ISBA, JULES-GL7, JULES-UKESM, and JULES-I impose complete snow cover or switch off their subgrid parameterizations, according to Menard et al. (2021). Among them, however, we identified the parameterization of snow cover fraction in SURFEX-ISBA, JULES-GL7, JULES-UKESM, and JULES-I, which concerns specific variables and illustrated appropriate location in the diagram in Figure 4.

The land surface model's newly added snow cover parameterization method reflects the sub-grid topography variation in CLM 5. Ma et al. (2019) used this method which considers the sub-grid unit's terrain characteristics to calculate the snow cover fraction. However, this method has a limitation due to only taking a variable called "elevation" into account as the standard deviation for the feature of the geomorphic setting. Roesch and Roeckner (2006) also measured snow cover fraction

https://doi.org/10.5194/tc-2021-319
Preprint. Discussion started: 30 November 2021

in the ECHAM climate model using the standard deviation of the sub-grid elevation and SWE. Douville et al. (1995) proposed a formula with the irregular snow cover distribution for the mountainous areas, including snow depth, roughness length, and the standard deviation of the subgrid orography (m).

Clark et al. (2011) presented a list of predictors related to the cause of spatial variation in snow depth according to spatial scale, as shown in Table 9. The list included both the elevation and slope among the significant predictors for snow temporal and spatial distribution. Since the spatial variation of snow depth is highly relevant with snow cover, we can apply essential predictors to the snow cover fraction parameterization. Anderson et al. (2014) also provided insights into the snow physics process that regulates the relationship between snow distribution and topographic characteristics and argued that snow cover correlates with altitude, aspect, canopy density, and snow accumulation/ablation. Besides, Mott et al. (2018) suggested that the characteristics of snow cover change according to the mountain range scale, the ridge, and the slope scale may differ. This idea provides worth variables considering when applying scales to interesting areas in LSMs. First, snow accumulation depends on the climate, elevation, and vegetation at the mountain-range scale (López-Moreno et al., 2008; Clark et al., 2011; Anderson et al., 2014). Especially, elevation is the most significant variable for precipitation pattern at the mountain range scale (Mott et al., 2018). Second, snow deposition patterns at the ridge-scale reveal more considerable spatial variability of snow or enhanced snow deposition over leeward slopes by preferential deposition of snowfall (Mott and Lehning, 2010; Gerber et al., 2017). Third, at the slope scale, the highest model resolutions show the snow redistribution processes such as saltation and turbulent suspension (Mott et al., 2018).

Noah LSM, CLM 5, and JULES calculates the land surface albedo by summing the ground albedo without snow and the snow albedo using the snow cover fraction. Other LSM models using the Noah LSM's snow albedo decay scheme were VIC and DHSVM. Livneh et al. (2010) introduced the parameter value of albedo decay parameterization. Storck (2000), Sun et al. (2019), and Malik et al. (2014) also enhanced this parameter to fit the characteristics of the study area. Furthermore, maximum snow albedo was approximately 0.6–0.95 in other LSMs and journal articles (Sproles et al., 2013; Verseghy, 1991; Wigmosta et al., 1994; Andreadis et al., 2009; Yang et al., 1997; Bartelt and Lehning, 2002). In Noah LSM, snow albedo is affected by snow cover; it affects the latent heat of the freezing rain, the heat flux of the snow surface, and the phase change heat flux for snow melting. Therefore, the maximum snow albedo is the main parameter of snow albedo parameterization, so setting the maximum snow albedo's optimal value is essential.

In addition to the HTESSEL, BATS, and CLASS models, ISBA includes a prognostic albedo scheme in which the previous snow albedo value affects the current snow albedo value. At first, CLASS did not consider the snow albedo changes according to the spectral range, similar to HTESSEL (Eqs. (k) and (l) in Table 5). Noah-MP also used this scheme (Wang et al., 2020). After that, CLASS applied the difference between visible and near-infrared snow albedo according to spectral range like CLM 5, BATS, JULES, and ISBA; it used an empirical formulation that has the difference between dry snow (Eqs. (n) and (o) in Table 5) and melting snow (Eqs. (p) and (q) in Table 5). Melton et al. (2019) used the spectral method instead of the empirical exponential decay function in order to apply the results of Wiscombe and Warren (1980) that the growth of snow particles, soot/dirt precipitation affects snow albedo. BATS's snow albedo parameterization method was actively accepted in CLASS, and there was a slight difference in applying to freshly fallen snow with a near-infrared value of 0.73, unlike BATS's 0.65. In

https://doi.org/10.5194/tc-2021-319
Preprint. Discussion started: 30 November 2021

addition, the structure of the equation reflecting the effect of the solar zenith angle was slightly different. The CLASS model in CLASSIC shows the most significant difference from other land surface models in that they reflected canopy albedo (Bartlett and Verseghy, 2015; Melton et al., 2020). In particular, CLASS has the lowest albedo bias among the JULES-I, JULES-GL7, JULES-UKESM, Surfex-ISBA, CLM 5, CLASS, and HTESSEL from Menard et al. (2021) (Figure 5). Thus, in future studies, the improvement of snow albedo simulation that reflects the effect of vegetation is crucial.

Since many LSMs calculate the snow depth as the SWE ratio to the snow density, it is vital to parameterize the new snow density affected by fresh snowfall. The new snow density's minimum value differed slightly depending on the type of LSM or the study area, so it was necessary to adjust the parameter value. In the snow density parameterization, although CLM 5, HTESSEL, and ISBA took wind and temperature into consideration when calculating the new snow density (Noah LSM, Noah-MP only considered temperature), various other variables may affect the new snow density.

Föhn (1976, 1985) raised the question of the representativeness of the measurement of the new snow depth in precipitation gauges in the mountains because they ignored the topographical characteristics such as the mountain peak, the wind-slope, and the leeward slope or depressions. Since records from rainfall gauges surrounded by valley plains help infer the depth of new snow depths over large areas (Föhn, 1976, 1985). Therefore, it is imperative to reflect the influence of topographic conditions' variation (elevation and slope) for mountainous areas' snow depth. Clark et al. (2011) proposed to derive snow depth by considering topographic variations such as wind slope vs. leeward slope, depression, crests, and the variation of critical elevation. Spatial variation of snow depth and temporal consistency of snow cover diversified due to snow freezing temperature, slope, aspect, and radiation. Hojatimalekshah et al. (2020) examined the relationship between tree canopy and snow depth and Kantzas et al. (2014) investigated the change of the snow regime according to vegetation dynamics through a ground model; these studies show that consideration of the vegetation effect is necessary for the snow parameterization method. Therefore, snow density parameterization regarding snow depth needs to include vegetation density, Leaf Area Index (LAI), Stem Area Index (SAI), vegetation type, and snow behavior in sheltered areas. In breif, geomorphic and vegetation-related variables can affect the spatial-temporal variation of the snow depth.

6 Conclusions

Examining the eight LSM's snow physics parameterizations allowed us to find each parameterization's vulnerabilities. Depending on the purpose of each LSM, we presented a comparison table so that readers can identify the variables already reflected in various LSMs which have enough information on snow-related schemes. We mainly focused on parameterization methods related to snow cover, snow albedo, and snow density. This study confirmed that snow cover, snow albedo, and snow density parameterization differ for each land surface model in terms of complexity and significant variables or parameters. The comparative analysis for each element is summarized as follows.

In the snow cover case, the snow decay scheme's parameterization method in CLM 5 considers the subgrid's topographical variation. Besides JULES, BATS, ISBA, and Noah MP used snow depth and roughness length for calculating the snow cover fraction. BATS and ISBA consider vegetation fraction, while Noah MP accounts for the melting factor using snow density.

https://doi.org/10.5194/tc-2021-319
Preprint. Discussion started: 30 November 2021

For the snow albedo parameterization, Noah LSM, CLM 5, and JULES use the snow cover fraction. Noah LSM, CLM 5, BATS, and HTESSEL used the maximum snow albedo for each vegetation type or applied the green vegetation fraction. Especially BATS, CLM 5, and JULES considered solar zenith angle, ice grain size to calculate snow albedo using direct & diffuse albedo and visible & near-infrared albedo. BATS and CLM 5 take into account the effect of impurities like dust or carbon on snow. CLASS does not consider solar zenith angle and was recently upgraded by calculating visible and near-infrared albedo for dry and melting snow, respectively.

In terms of snow density, while Noah LSM and Noah-MP consider only temperature, HTESSEL, CLM 5, and ISBA reflect temperature and wind to parameterize the density of new snowfall. ISBA and JULES include the internal snow processes such as vertical stress, snow temperature, and snow viscosity. In particular, ISBA accounts for the wind-driven snow compaction precisely. BATS calculates snow density using the growth of snow particle size and the accumulation of dust and soot. CLASS calculates the maximum snow density as a function of snow depth, which increases exponentially over time with wet snow. Noah LSM, BATS, CLASS, Noah-MP, HTESSEL, and CLM 5 considers SWE or snowfall rate and snow density for parameterizing snow depth, and HTESSEL and CLM 5 use the snow cover fraction additionally to the snow depth parameterization.

We suggested what variables need to be taken into account to properly reflect the snow's physical properties in the future outlook section. In particular, at a high-resolution spatio-temporal scale, we highlight the importance of geomorphic and vegetation conditions in snow parameterization. First, topographic features such as slope aspect, slope gradient, and altitude have great importance in snow ground physics. Second, we found that vegetation-related factors such as vegetation density, vegetation type, vegetation cover fraction, LAI, and SAI are crucial for snow parameterization at the local scale. In future LSM improvement studies, we recommended a parameterization method that considers the topography and vegetation characteristics.

Author contributions. Seon Ki Park designed the study and conceptualized the paper. Won Young Lee contributed to writing the original draft. Hyeon-ju Gim and Seon Ki Park reviewed and edited the article.

Competing interests. The authors declare that they have no conflict of interest.

Acknowledgements. The authors acknowledge their funding resources. This research was supported by the Basic Science Research Program through the National Research Foundation of Korea (NRF) funded by the Ministry of Education (2018R1A6A1A08025520 & 2021R1I1A1A01059711). This research is supported by the Development of Numerical Weather Prediction and Data Application Techniques, Numerical Modeling Center, Korea Meteorological Administration (NTIS-1365003428).

https://doi.org/10.5194/tc-2021-319
Preprint. Discussion started: 30 November 2021

References

Aguado, E.: Radiation Balances of Melting Snow Covers at an Open Site in the Central Sierra Nevada, California, Water Resources Research, 21, 1649–1654, https://doi.org/10.1029/wr021i011p01649, 1985.

Anderson, B. T., McNamara, J. P., Marshall, H.-P., and Flores, A. N.: Insights into the physical processes controlling correlations between snow distribution and terrain properties, Water Resources Research, 50, 4545–4563, https://doi.org/10.1002/2013wr013714, 2014.

Anderson, E.: National Weather Service River Forecast System: Snow Accumulation and Ablation Model, NOAA technical memorandum NWS HYDRO, U.S. Department of Commerce, National Oceanic and Atmospheric Administration, National Weather Service, https://books.google.co.kr/books?id=Vi1rAQAACAAJ, 1973.

Anderson, J. R., Hardy, E. E., Roach, J. T., and Witmer, R. E.: A land use and land cover classification system for use with remote sensor data, https://doi.org/10.3133/pp964, 1976.

Anderton, S. P., White, S. M., and Alvera, B.: Evaluation of spatial variability in snow water equivalent for a high mountain catchment, Hydrological Processes, 18, 435–453, https://doi.org/10.1002/hyp.1319, 2004.

Andreadis, K. M., Storck, P., and Lettenmaier, D. P.: Modeling snow accumulation and ablation processes in forested environments, Water Resources Research, 45, https://doi.org/10.1029/2008wr007042, 2009.

Armstrong, R. and Brun, E.: Introduction, in: Snow and Climate: Physical Processes, Surface Energy Exchange and Modeling, edited by Armstrong, R. and Brun, E., chap. 1, pp. 1–11, Cambridge University Press, 2008.

Baker, D. G., Ruschy, D. L., and Wall, D. B.: The Albedo Decay of Prairie Snows, Journal of Applied Meteorology, 29, 179–187, https://doi.org/10.1175/1520-0450(1990)029<0179:tadops>2.0.co;2, 1990.

Balk, B. and Elder, K.: Combining binary decision tree and geostatistical methods to estimate snow distribution in a mountain watershed, Water Resources Research, 36, 13–26, https://doi.org/10.1029/1999wr900251, 2000.

Barlage, M., Chen, F., Tewari, M., Ikeda, K., Gochis, D., Dudhia, J., Rasmussen, R., Livneh, B., Ek, M., and Mitchell, K.: Noah land surface model modifications to improve snowpack prediction in the Colorado Rocky Mountains, Journal of Geophysical Research, 115, https://doi.org/10.1029/2009jd013470, 2010.

Bartelt, P. and Lehning, M.: A physical SNOWPACK model for the Swiss avalanche warning, Cold Regions Science and Technology, 35, 123–145, https://doi.org/10.1016/s0165-232x(02)00074-5, 2002.

Bartlett, P. A. and Verseghy, D. L.: Modified treatment of intercepted snow improves the simulated forest albedo in the Canadian Land Surface Scheme, Hydrological Processes, 29, 3208–3226, https://doi.org/10.1002/hyp.10431, 2015.

Bartlett, P. A., MacKay, M. D., and Verseghy, D. L.: Modified snow algorithms in the Canadian land surface scheme: Model runs and sensitivity analysis at three boreal forest stands, Atmosphere-Ocean, 44, 207–222, https://doi.org/10.3137/ao.440301, 2006.

Best, M. J., Pryor, M., Clark, D. B., Rooney, G. G., Essery, R. L. H., Ménard, C. B., Edwards, J. M., Hendry, M. A., Porson, A., Gedney, N., Mercado, L. M., Sitch, S., Blyth, E., Boucher, O., Cox, P. M., Grimmond, C. S. B., and Harding, R. J.: The Joint UK Land Environment Simulator (JULES), model description – Part 1: Energy and water fluxes, 4, 677–699, https://doi.org/10.5194/gmd-4-677-2011, 2011.

Betts, A. K. and Ball, J. H.: Albedo over the boreal forest, Journal of Geophysical Research: Atmospheres, 102, 28 901–28 909, https://doi.org/10.1029/96jd03876, 1997.

Blöschl, G. and Kirnbauer, R.: An analysis of snow cover patterns in a small alpine catchment, Hydrological Processes, 6, 99–109, https://doi.org/10.1002/hyp.3360060109, 1992.

https://doi.org/10.5194/tc-2021-319
Preprint. Discussion started: 30 November 2021

Bohren, C. F. and Barkstrom, B. R.: Theory of the optical properties of snow, 79, 4527–4535, https://doi.org/10.1029/jc079i030p04527, 1974.

Bonan, G.: A Land Surface Model (LSM Version 1.0) for Ecological, Hydrological, and Atmospheric Studies: Technical Description and User's Guide, Tech. rep., https://doi.org/10.5065/D6DF6P5X, 1996.

Bowling, L. C., Lettenmaier, D. P., Nijssen, B., Graham, L., Clark, D. B., Maayar, M. E., Essery, R., Goers, S., Gusev, Y. M., Habets, F., van den Hurk, B., Jin, J., Kahan, D., Lohmann, D., Ma, X., Mahanama, S., Mocko, D., Nasonova, O., Niu, G.-Y., Samuelsson, P., Shmakin, A. B., Takata, K., Verseghy, D., Viterbo, P., Xia, Y., Xue, Y., and Yang, Z.-L.: Simulation of high-latitude hydrological processes in the Torne–Kalix basin: PILPS Phase 2(e), Global and Planetary Change, 38, 1–30, https://doi.org/10.1016/s0921-8181(03)00003-1, 2003.

Brown, R., Bartlett, P., MacKay, M., and Verseghy, D.: Evaluation of snow cover in CLASS for SnowMIP, Atmosphere-Ocean, 44, 223–238, https://doi.org/10.3137/ao.440302, 2006.

Brown, R. D., Brasnett, B., and Robinson, D.: Gridded North American monthly snow depth and snow water equivalent for GCM evaluation, Atmosphere-Ocean, 41, 1–14, https://doi.org/10.3137/ao.410101, 2003.

Brun, E., . Martin, Simon, V., Gendre, C., and Coleou, C.: An Energy and Mass Model of Snow Cover Suitable for Operational Avalanche Forecasting, Journal of Glaciology, 35, 333–342, https://doi.org/10.3189/s0022143000009254, 1989.

Brun, E., David, P., Sudul, M., and Brunot, G.: A numerical model to simulate snow-cover stratigraphy for operational avalanche forecasting, Journal of Glaciology, 38, 13–22, https://doi.org/10.3189/s0022143000009552, 1992.

Brun, E., Martin, E., and Spiridonov, V.: Coupling a multi-layered snow model with a GCM, 25, 66–72, https://doi.org/10.3189/s0260305500013811, 1997.

Brun, E., Yang, Z.-L., Essery, R., and Cohen, J.: Snow-cover parameterization and modeling, in: Snow and Climate: Physical Processes, Surface Energy Exchange and Modeling, edited by Armstrong, R. and Brun, E., chap. 4, pp. 125–180, Cambridge University Press, 2008.

Clark, M. P., Hendrikx, J., Slater, A. G., Kavetski, D., Anderson, B., Cullen, N. J., Kerr, T., Örn Hreinsson, E., and Woods, R. A.: Representing spatial variability of snow water equivalent in hydrologic and land-surface models: A review, Water Resources Research, 47, https://doi.org/10.1029/2011wr010745, 2011.

Colbeck, S. C.: Theory of metamorphism of wet snow. CRREL Res. Rep. 313., Tech. rep., Cold Regions Research and Engineering Laboratory (U.S.), https://hdl.handle.net/11681/5894, 1973.

Cuffey, K. M., P. W. S. B.: The physics of glaciers, Butterworth-Heinemann/Elsevier, Burlington, MA, 2010.

Danabasoglu, G., Lamarque, J.-F., Bacmeister, J., Bailey, D. A., DuVivier, A. K., Edwards, J., Emmons, L. K., Fasullo, J., Garcia, R., Gettelman, A., Hannay, C., Holland, M. M., Large, W. G., Lauritzen, P. H., Lawrence, D. M., Lenaerts, J. T. M., Lindsay, K., Lipscomb, W. H., Mills, M. J., Neale, R., Oleson, K. W., Otto-Bliesner, B., Phillips, A. S., Sacks, W., Tilmes, S., Kampenhout, L., Vertenstein, M., Bertini, A., Dennis, J., Deser, C., Fischer, C., Fox-Kemper, B., Kay, J. E., Kinnison, D., Kushner, P. J., Larson, V. E., Long, M. C., Mickelson, S., Moore, J. K., Nienhouse, E., Polvani, L., Rasch, P. J., and Strand, W. G.: The Community Earth System Model Version 2 (CESM2), Journal of Advances in Modeling Earth Systems, 12, https://doi.org/10.1029/2019ms001916, 2020.

Dawson, N., Broxton, P., and Zeng, X.: A New Snow Density Parameterization for Land Data Initialization, Journal of Hydrometeorology, 18, 197–207, https://doi.org/10.1175/jhm-d-16-0166.1, 2017.

Decharme, B., Brun, E., Boone, A., Delire, C., Moigne, P. L., and Morin, S.: Impacts of snow and organic soils parameterization on northern Eurasian soil temperature profiles simulated by the ISBA land surface model, 10, 853–877, https://doi.org/10.5194/tc-10-853-2016, 2016.

Decharme, B., Delire, C., Minvielle, M., Colin, J., Vergnes, J.-P., Alias, A., Saint-Martin, D., Séférian, R., Sénési, S., and Voldoire, A.: Recent Changes in the ISBA-CTRIP Land Surface System for Use in the CNRM-CM6 Climate Model and in Global Off-Line Hydrological Applications, 11, 1207–1252, https://doi.org/10.1029/2018ms001545, 2019.

Dickinson, R., Henderson-Sellers, A., Kennedy, P., and Wilson, M.: Biosphere-atmosphere Transfer Scheme (BATS) for the NCAR Community Climate Model, Tech. rep., https://doi.org/10.5065/D6668B58, 1986.

Dickinson, R., Henderson-Sellers, A., and Kennedy, P.: Biosphere-atmosphere Transfer Scheme (BATS) Version 1e as Coupled to the NCAR Community Climate Model, Tech. rep., https://doi.org/10.5065/D67W6959, 1993.

Dirmhirn, I. and Eaton, F. D.: Some Characteristics of the Albedo of Snow, Journal of Applied Meteorology, 14, 375–379, https://doi.org/10.1175/1520-0450(1975)014<0375:scotao>2.0.co;2, 1975.

Douville, H., Royer, J. F., and Mahfouf, J. F.: A new snow parameterization for the Météo-France climate model, Climate Dynamics, 12, 21–35, https://doi.org/10.1007/bf00208760, 1995.

Dutra, E., Balsamo, G., Viterbo, P., Miranda, P., Beljaars, A., Schär, C., and Elder, K.: New snow scheme in HTESSEL: description and offline validation, Technical memorandum, p. 25, https://doi.org/10.21957/98x9mrv1y, 2009.

Ekici, A., Beer, C., Hagemann, S., Boike, J., Langer, M., and Hauck, C.: Simulating high-latitude permafrost regions by the JSBACH terrestrial ecosystem model, Geoscientific Model Development, 7, 631–647, https://doi.org/10.5194/gmd-7-631-2014, 2014.

Elder, K., Dozier, J., and Michaelsen, J.: Snow accumulation and distribution in an Alpine Watershed, Water Resources Research, 27, 1541–1552, https://doi.org/10.1029/91wr00506, 1991.

Elder, K., Rosenthal, W., and Davis, R. E.: Estimating the spatial distribution of snow water equivalence in a montane watershed, Hydrological Processes, 12, 1793–1808, https://doi.org/10.1002/(sici)1099-1085(199808/09)12:10/11<1793::aid-hyp695>3.0.co;2-k, 1998.

Erickson, T. A., Williams, M. W., and Winstral, A.: Persistence of topographic controls on the spatial distribution of snow in rugged mountain terrain, Colorado, United States, Water Resources Research, 41, https://doi.org/10.1029/2003wr002973, 2005.

Essery, R. and Pomeroy, J.: Vegetation and Topographic Control of Wind-Blown Snow Distributions in Distributed and Aggregated Simulations for an Arctic Tundra Basin, Journal of Hydrometeorology, 5, 735–744, https://doi.org/10.1175/1525-7541(2004)005<0735:vatcow>2.0.co;2, 2004.

Essery, R., Rutter, N., Pomeroy, J., Baxter, R., Stähli, M., Gustafsson, D., Barr, A., Bartlett, P., and Elder, K.: SNOWMIP2: An Evaluation of Forest Snow Process Simulations, Bulletin of the American Meteorological Society, 90, 1120–1136, https://doi.org/10.1175/2009bams2629.1, 2009.

Etchevers, P., Martin, E., Brown, R., Fierz, C., Lejeune, Y., Bazile, E., Boone, A., Dai, Y.-J., Essery, R., Fernandez, A., Gusev, Y., Jordan, R., Koren, V., Kowalczyk, E., Nasonova, N. O., Pyles, R. D., Schlosser, A., Shmakin, A. B., Smirnova, T. G., Strasser, U., Verseghy, D., Yamazaki, T., and Yang, Z.-L.: Validation of the energy budget of an alpine snowpack simulated by several snow models (Snow MIP project), Annals of Glaciology, 38, 150–158, https://doi.org/10.3189/172756404781814825, 2004.

Faria, D. A., Pomeroy, J. W., and Essery, R. L. H.: Effect of covariance between ablation and snow water equivalent on depletion of snow-covered area in a forest, Hydrological Processes, 14, 2683–2695, https://doi.org/10.1002/1099-1085(20001030)14:15<2683::aid-hyp86>3.0.co;2-n, 2000.

Fernandes, R., Prevost, C., Canisius, F., Leblanc, S. G., Maloley, M., Oakes, S., Holman, K., and Knudby, A.: Monitoring snow depth change across a range of landscapes with ephemeral snowpacks using structure from motion applied to lightweight unmanned aerial vehicle videos, The Cryosphere, 12, 3535–3550, https://doi.org/10.5194/tc-12-3535-2018, 2018.

Flanner, M. G.: Snowpack radiative heating: Influence on Tibetan Plateau climate, Geophysical Research Letters, 32, https://doi.org/10.1029/2004gl022076, 2005.

Flanner, M. G., Zender, C. S., Randerson, J. T., and Rasch, P. J.: Present-day climate forcing and response from black carbon in snow, Journal of Geophysical Research, 112, https://doi.org/10.1029/2006jd008003, 2007.

Föhn, P. M. B.: Representativeness of precipitation measurements in mountainous areas. In Poc. of the Joint Scientific Meeting on Mountain Meteorology and Biometeorology, June 10–14, 1976, Interlaken, Switzerland, Bulletin of the American Meteorological Society, 57, 267–285, https://doi.org/10.1175/1520-0477-57.2.267, 1976.

Föhn, P. M. B.: Besonderheiten des Schneeniederschlages, In Der Niederschlag in der Schweiz. Beitr. Geol. Schweiz – Hydrol., 31, 87–96, 1985.

Gerber, F., Lehning, M., Hoch, S. W., and Mott, R.: A close-ridge small-scale atmospheric flow field and its influence on snow accumulation, Journal of Geophysical Research: Atmospheres, 122, 7737–7754, https://doi.org/10.1002/2016jd026258, 2017.

Gold, L. W.: Changes in a Shallow Snow Cover Subject to a Temperate Climate, Journal of Glaciology, 3, 218–222, https://doi.org/10.3189/s002214300002428x, 1958.

Gottlib, L.: A general runoff model for snow-covered and glacierized basins, in: 6TH Nordic Hydrological Conference, Vemadolen, Sweden, pp. 172–177, 1980.

He, H., He, D., Jin, J., Smits, K. M., Dyck, M., Wu, Q., Si, B., and Lv, J.: Room for improvement: A review and evaluation of 24 soil thermal conductivity parameterization schemes commonly used in land-surface, hydrological, and soil-vegetation-atmosphere transfer models, Earth-Science Reviews, 211, 103 419, https://doi.org/10.1016/j.earscirev.2020.103419, 2020.

Hedrick, A., Marshall, H.-P., Winstral, A., Elder, K., Yueh, S., and Cline, D.: Independent evaluation of the SNODAS snow depth product using regional-scale lidar-derived measurements, The Cryosphere, 9, 13–23, https://doi.org/10.5194/tc-9-13-2015, 2015.

Hedstrom, N. R. and Pomeroy, J. W.: Measurements and modelling of snow interception in the boreal forest, 12, 1611–1625, https://doi.org/10.1002/(sici)1099-1085(199808/09)12:10/11<1611::aid-hyp684>3.0.co;2-4, 1998.

Hojatimalekshah, A., Uhlmann, Z., Glenn, N. F., Hiemstra, C. A., Tennant, C. J., Graham, J. D., Spaete, L., Gelvin, A., Marshall, H.-P., McNamara, J., and Enterkine, J.: Tree canopy and snow depth relationships at fine scales with terrestrial laser scanning, https://doi.org/10.5194/tc-2020-277, 2020.

Hong, S.-Y., Kwon, Y. C., Kim, T.-H., Kim, J.-E. E., Choi, S.-J., Kwon, I.-H., Kim, J., Lee, E.-H., Park, R.-S., and Kim, D.-I.: The Korean Integrated Model (KIM) System for Global Weather Forecasting, Asia-Pacific Journal of Atmospheric Sciences, 54, 267–292, https://doi.org/10.1007/s13143-018-0028-9, 2018.

Jin, Y., Gao, F., Schaaf, C., Li, X., Strahler, A., Bruegge, C., and Martonchik, J.: Improving MODIS surface BRDF/Albedo retrieval with MISR multiangle observations, IEEE Transactions on Geoscience and Remote Sensing, 40, 1593–1604, https://doi.org/10.1109/tgrs.2002.801145, 2002.

Jordan, R. E., Andreas, E. L., and Makshtas, A. P.: Heat budget of snow-covered sea ice at North Pole 4, Journal of Geophysical Research: Oceans, 104, 7785–7806, https://doi.org/10.1029/1999jc900011, 1999.

Jordan, R. E., Albert, M. R., and Brun, E.: Physical processes within the snow cover and their parameterization, in: Snow and Climate: Physical Processes, Surface Energy Exchange and Modeling, edited by Armstrong, R. and Brun, E., chap. 2, pp. 12–69, Cambridge University Press, 2008.

Kantzas, E., Quegan, S., Lomas, M., and Zakharova, E.: Evaluation of the snow regime in dynamic vegetation land surface models using field measurements, The Cryosphere, 8, 487–502, https://doi.org/10.5194/tc-8-487-2014, 2014.

Koren, V., Schaake, J., Mitchell, K., Duan, Q.-Y., Chen, F., and Baker, J. M.: A parameterization of snowpack and frozen ground intended for NCEP weather and climate models, Journal of Geophysical Research: Atmospheres, 104, 19 569–19 585, https://doi.org/10.1029/1999jd900232, 1999.

Krinner, G., Derksen, C., Essery, R., Flanner, M., Hagemann, S., Clark, M., Hall, A., Rott, H., Brutel-Vuilmet, C., Kim, H., Ménard, C. B., Mudryk, L., Thackeray, C., Wang, L., Arduini, G., Balsamo, G., Bartlett, P., Boike, J., Boone, A., Chéruy, F., Colin, J., Cuntz, M., Dai, Y., Decharme, B., Derry, J., Ducharne, A., Dutra, E., Fang, X., Fierz, C., Ghattas, J., Gusev, Y., Haverd, V., Kontu, A., Lafaysse, M., Law, R., Lawrence, D., Li, W., Marke, T., Marks, D., Ménégoz, M., Nasonova, O., Nitta, T., Niwano, M., Pomeroy, J., Raleigh, M. S., Schaedler, G., Semenov, V., Smirnova, T. G., Stacke, T., Strasser, U., Svenson, S., Turkov, D., Wang, T., Wever, N., Yuan, H., Zhou, W., and Zhu, D.: ESM-SnowMIP: assessing snow models and quantifying snow-related climate feedbacks, Geoscientific Model Development, 11, 5027–5049, https://doi.org/10.5194/gmd-11-5027-2018, 2018.

Lapena, D. R. and Martz, L. W.: An investigation of the spatial association between snow depth and topography in a Prairie agricultural landscape using digital terrain analysis, Journal of Hydrology, 184, 277–298, https://doi.org/10.1016/0022-1694(95)02975-3, 1996.

Lawrence, D., Fisher, R., Koven, C., Oleson, K., Swenson, S., and Vertenstein, M.: Technical description of version 5.0 of the community land model (CLM), Tech. rep., National Center for Atmospheric Research (NCAR), http://www.cesm.ucar.edu/models/cesm2/land/CLM50_Tech_Note.pdf, 2018.

Lawrence, D. M., Fisher, R. A., Koven, C. D., Oleson, K. W., Swenson, S. C., Bonan, G., Collier, N., Ghimire, B., Kampenhout, L., Kennedy, D., Kluzek, E., Lawrence, P. J., Li, F., Li, H., Lombardozzi, D., Riley, W. J., Sacks, W. J., Shi, M., Vertenstein, M., Wieder, W. R., Xu, C., Ali, A. A., Badger, A. M., Bisht, G., Broeke, M., Brunke, M. A., Burns, S. P., Buzan, J., Clark, M., Craig, A., Dahlin, K., Drewniak, B., Fisher, J. B., Flanner, M., Fox, A. M., Gentine, P., Hoffman, F., Keppel-Aleks, G., Knox, R., Kumar, S., Lenaerts, J., Leung, L. R., Lipscomb, W. H., Lu, Y., Pandey, A., Pelletier, J. D., Perket, J., Randerson, J. T., Ricciuto, D. M., Sanderson, B. M., Slater, A., Subin, Z. M., Tang, J., Thomas, R. Q., Martin, M. V., and Zeng, X.: The Community Land Model Version 5: Description of New Features, Benchmarking, and Impact of Forcing Uncertainty, Journal of Advances in Modeling Earth Systems, 11, 4245–4287, https://doi.org/10.1029/2018ms001583, 2019.

Lawrence, P. J. and Chase, T. N.: Representing a new MODIS consistent land surface in the Community Land Model (CLM 3.0), Journal of Geophysical Research, 112, https://doi.org/10.1029/2006jg000168, 2007.

Li, C., Lu, H., Yang, K., Wright, J. S., Yu, L., Chen, Y., Huang, X., and Xu, S.: Evaluation of the Common Land Model (CoLM) from the Perspective of Water and Energy Budget Simulation: Towards Inclusion in CMIP6, Atmosphere, 8, 141, https://doi.org/10.3390/atmos8080141, 2017.

Liston, G. E. and Elder, K.: A Distributed Snow-Evolution Modeling System (SnowModel), Journal of Hydrometeorology, 7, 1259–1276, https://doi.org/10.1175/jhm548.1, 2006.

Livneh, B., Xia, Y., Mitchell, K. E., Ek, M. B., and Lettenmaier, D. P.: Noah LSM Snow Model Diagnostics and Enhancements, Journal of Hydrometeorology, 11, 721–738, https://doi.org/10.1175/2009jhm1174.1, 2010.

Longley, R. W.: Snow Depth and Snow Density at Resolute, Northwest Territories, Journal of Glaciology, 3, 733–738, https://doi.org/10.3189/s0022143000018037, 1960.

López-Moreno, J. I., Goyette, S., Beniston, M., and Alvera, B.: Sensitivity of the snow energy balance to climatic changes: prediction of snowpack in the Pyrenees in the 21st century, Climate Research, 36, 203–217, https://doi.org/10.3354/cr00747, 2008.

López-Moreno, J. I., Fassnacht, S. R., Beguería, S., and Latron, J. B. P.: Variability of snow depth at the plot scale: implications for mean depth estimation and sampling strategies, The Cryosphere, 5, 617–629, https://doi.org/10.5194/tc-5-617-2011, 2011.

https://doi.org/10.5194/tc-2021-319
Preprint. Discussion started: 30 November 2021

Luce, C. H., Tarboton, D. G., and Cooley, K. R.: The influence of the spatial distribution of snow on basin-averaged snowmelt, Hydrological Processes, 12, 1671–1683, https://doi.org/10.1002/(sici)1099-1085(199808/09)12:10/11<1671::aid-hyp688>3.0.co;2-n, 1998.

Ma, X., Jin, J., Liu, J., and Niu, G.-Y.: An improved vegetation emissivity scheme for land surface modeling and its impact on snow cover simulations, Climate Dynamics, 53, 6215–6226, https://doi.org/10.1007/s00382-019-04924-9, 2019.

Malik, M. J., van der Velde, R., Vekerdy, Z., and Su, Z.: Improving modeled snow albedo estimates during the spring melt season, Journal of Geophysical Research: Atmospheres, 119, 7311–7331, https://doi.org/10.1002/2013jd021344, 2014.

Marchand, W.-D. and nund Killingtveit: Statistical probability distribution of snow depth at the model sub-grid cell spatial scale, Hydrological Processes, 19, 355–369, https://doi.org/10.1002/hyp.5543, 2005.

Masson, V., Moigne, P. L., Martin, E., Faroux, S., Alias, A., Alkama, R., Belamari, S., Barbu, A., Boone, A., Bouyssel, F., Brousseau, P., Brun, E., Calvet, J.-C., Carrer, D., Decharme, B., Delire, C., Donier, S., Essaouini, K., Gibelin, A.-L., Giordani, H., Habets, F., Jidane, M., Kerdraon, G., Kourzeneva, E., Lafaysse, M., Lafont, S., Brossier, C. L., Lemonsu, A., Mahfouf, J.-F., Marguinaud, P., Mokhtari, M., Morin, S., Pigeon, G., Salgado, R., Seity, Y., Taillefer, F., Tanguy, G., Tulet, P., Vincendon, B., Vionnet, V., and Voldoire, A.: The SURFEXv7.2 land and ocean surface platform for coupled or offline simulation of earth surface variables and fluxes, Geoscientific Model Development, 6, 929–960, https://doi.org/10.5194/gmd-6-929-2013, 2013.

McCartney, S. E., Carey, S. K., and Pomeroy, J. W.: Intra-basin variability of snowmelt water balance calculations in a subarctic catchment, Hydrological Processes, 20, 1001–1016, https://doi.org/10.1002/hyp.6125, 2006.

Melton, J. R. and Arora, V. K.: Competition between plant functional types in the Canadian Terrestrial Ecosystem Model (CTEM) v. 2.0, Geoscientific Model Development, 9, 323–361, https://doi.org/10.5194/gmd-9-323-2016, 2016.

Melton, J. R., Verseghy, D. L., Sospedra-Alfonso, R., and Gruber, S.: Improving permafrost physics in the coupled Canadian Land Surface Scheme (v.3.6.2) and Canadian Terrestrial Ecosystem Model (v.2.1) (CLASS-CTEM), Geoscientific Model Development, 12, 4443–4467, https://doi.org/10.5194/gmd-12-4443-2019, 2019.

Melton, J. R., Arora, V. K., Wisernig-Cojoc, E., Seiler, C., Fortier, M., Chan, E., and Teckentrup, L.: CLASSIC v1.0: the open-source community successor to the Canadian Land Surface Scheme (CLASS) and the Canadian Terrestrial Ecosystem Model (CTEM) – Part 1: Model framework and site-level performance, Geoscientific Model Development, 13, 2825–2850, https://doi.org/10.5194/gmd-13-2825-2020, 2020.

Menard, C. B., Essery, R., Krinner, G., Arduini, G., Bartlett, P., Boone, A., Brutel-Vuilmet, C., Burke, E., Cuntz, M., Dai, Y., Decharme, B., Dutra, E., Fang, X., Fierz, C., Gusev, Y., Hagemann, S., Haverd, V., Kim, H., Lafaysse, M., Marke, T., Nasonova, O., Nitta, T., Niwano, M., Pomeroy, J., Schädler, G., Semenov, V. A., Smirnova, T., Strasser, U., Swenson, S., Turkov, D., Wever, N., and Yuan, H.: Scientific and Human Errors in a Snow Model Intercomparison, Bulletin of the American Meteorological Society, 102, E61–E79, https://doi.org/10.1175/bams-d-19-0329.1, 2021.

Menary, M. B., Kuhlbrodt, T., Ridley, J., Andrews, M. B., Dimdore-Miles, O. B., Deshayes, J., Eade, R., Gray, L., Ineson, S., Mignot, J., Roberts, C. D., Robson, J., Wood, R. A., and Xavier, P.: Preindustrial Control Simulations With HadGEM3-GC3.1 for CMIP6, Journal of Advances in Modeling Earth Systems, https://doi.org/10.1029/2018ms001495, 2018.

Moody, E. G., King, M. D., Schaaf, C. B., Hall, D. K., and Platnick, S.: Northern Hemisphere five-year average (2000–2004) spectral albedos of surfaces in the presence of snow: Statistics computed from Terra MODIS land products, Remote Sensing of Environment, 111, 337–345, https://doi.org/10.1016/j.rse.2007.03.026, 2007.

Mott, R. and Lehning, M.: Meteorological Modeling of Very High-Resolution Wind Fields and Snow Deposition for Mountains, Journal of Hydrometeorology, 11, 934–949, https://doi.org/10.1175/2010jhm1216.1, 2010.

https://doi.org/10.5194/tc-2021-319
Preprint. Discussion started: 30 November 2021

Mott, R., Vionnet, V., and Grünewald, T.: The Seasonal Snow Cover Dynamics: Review on Wind-Driven Coupling Processes, Frontiers in Earth Science, 6, https://doi.org/10.3389/feart.2018.00197, 2018.

Mölders, N., Luijting, H., and Sassen, K.: Use of atmospheric radiation measurement program data from Barrow, Alaska, for evaluation and development of snow-albedo parameterizations, Meteorology and Atmospheric Physics, 99, 199–219, https://doi.org/10.1007/s00703-007-0271-6, 2007.

Niu, G.-Y. and Yang, Z.-L.: An observation-based formulation of snow cover fraction and its evaluation over large North American river basins, 112, https://doi.org/10.1029/2007jd008674, 2007.

Niu, G.-Y., Yang, Z.-L., Mitchell, K. E., Chen, F., Ek, M. B., Barlage, M., Kumar, A., Manning, K., Niyogi, D., Rosero, E., Tewari, M., and Xia, Y.: The community Noah land surface model with multiparameterization options (Noah-MP): 1. Model description and evaluation with local-scale measurements, 116, https://doi.org/10.1029/2010jd015139, 2011.

Pedersen, C. A. and Winther, J.-G.: Intercomparison and validation of snow albedo parameterization schemes in climate models, Climate Dynamics, 25, 351–362, https://doi.org/10.1007/s00382-005-0037-0, 2005.

Pitman, A. and Henderson-Sellers, A.: Recent progress and results from the project for the intercomparison of landsurface parameterization schemes, Journal of Hydrology, 212-213, 128–135, https://doi.org/10.1016/s0022-1694(98)00206-6, 1998.

Pomeroy, J. W., Gray, D. M., Hedstrom, N. R., and Janowicz, J. R.: Prediction of seasonal snow accumulation in cold climate forests, Hydrological Processes, 16, 3543–3558, https://doi.org/10.1002/hyp.1228, 2002.

Pomeroy, J. W., Bewley, D. S., Essery, R. L. H., Hedstrom, N. R., Link, T., Granger, R. J., Sicart, J. E., Ellis, C. R., and Janowicz, J. R.: Shrub tundra snowmelt, Hydrological Processes, 20, 923–941, https://doi.org/10.1002/hyp.6124, 2006.

Reick, C. H., Gayler, V., Goll, D., Hagemann, S., Heidkamp, M., Nabel, J. E. M. S., Raddatz, T., Roeckner, E., Schnur, R., and Wilkenskjeld, S.: JSBACH 3 - The land component of the MPI Earth System Model: documentation of version 3.2, https://doi.org/10.17617/2.3279802, 2021.

Robinson, D. A. and Kukla, G.: Albedo of a Dissipating Snow Cover, Journal of Climate and Applied Meteorology, 23, 1626–1634, https://doi.org/10.1175/1520-0450(1984)023<1626:aoadsc>2.0.co;2, 1984.

Roesch, A. and Roeckner, E.: Assessment of Snow Cover and Surface Albedo in the ECHAM5 General Circulation Model, Journal of Climate, 19, 3828–3843, https://doi.org/10.1175/jcli3825.1, 2006.

Roesch, A., Wild, M., Gilgen, H., and Ohmura, A.: A new snow cover fraction parametrization for the ECHAM4 GCM, Climate Dynamics, 17, 933–946, https://doi.org/10.1007/s003820100153, 2001.

Rutter, N., Essery, R., Pomeroy, J., Altimir, N., Andreadis, K., Baker, I., Barr, A., Bartlett, P., Boone, A., Deng, H., Douville, H., Dutra, E., Elder, K., Ellis, C., Feng, X., Gelfan, A., Goodbody, A., Gusev, Y., Gustafsson, D., Hellström, R., Hirabayashi, Y., Hirota, T., Jonas, T., Koren, V., Kuragina, A., Lettenmaier, D., Li, W.-P., Luce, C., Martin, E., Nasonova, O., Pumpanen, J., Pyles, R. D., Samuelsson, P., Sandells, M., Schädler, G., Shmakin, A., Smirnova, T. G., Stähli, M., Stöckli, R., Strasser, U., Su, H., Suzuki, K., Takata, K., Tanaka, K., Thompson, E., Vesala, T., Viterbo, P., Wiltshire, A., Xia, K., Xue, Y., and Yamazaki, T.: Evaluation of forest snow processes models (SnowMIP2), Journal of Geophysical Research, 114, https://doi.org/10.1029/2008jd011063, 2009.

Schaaf, C. B., Gao, F., Strahler, A. H., Lucht, W., Li, X., Tsang, T., Strugnell, N. C., Zhang, X., Jin, Y., Muller, J.-P., Lewis, P., Barnsley, M., Hobson, P., Disney, M., Roberts, G., Dunderdale, M., Doll, C., d'Entremont, R. P., Hu, B., Liang, S., Privette, J. L., and Roy, D.: First operational BRDF, albedo nadir reflectance products from MODIS, Remote Sensing of Environment, 83, 135–148, https://doi.org/10.1016/s0034-4257(02)00091-3, 2002.

https://doi.org/10.5194/tc-2021-319
Preprint. Discussion started: 30 November 2021

Sellar, A. A., Jones, C. G., Mulcahy, J. P., Tang, Y., Yool, A., Wiltshire, A., O'Connor, F. M., Stringer, M., Hill, R., Palmieri, J., Woodward, S., Mora, L., Kuhlbrodt, T., Rumbold, S. T., Kelley, D. I., Ellis, R., Johnson, C. E., Walton, J., Abraham, N. L., Andrews, M. B., Andrews, T., Archibald, A. T., Berthou, S., Burke, E., Blockley, E., Carslaw, K., Dalvi, M., Edwards, J., Folberth, G. A., Gedney, N., Griffiths, P. T., Harper, A. B., Hendry, M. A., Hewitt, A. J., Johnson, B., Jones, A., Jones, C. D., Keeble, J., Liddicoat, S., Morgenstern, O., Parker, R. J., Predoi, V., Robertson, E., Siahaan, A., Smith, R. S., Swaminathan, R., Woodhouse, M. T., Zeng, G., and Zerroukat, M.: UKESM1: Description and Evaluation of the U.K. Earth System Model, Journal of Advances in Modeling Earth Systems, 11, 4513–4558, https://doi.org/10.1029/2019ms001739, 2019.

Shook, K. and Gray, D. M.: Small-Scale Spaial Structure of Shallow Snowcovers, Hydrological Processes, 10, 1283–1292, https://doi.org/10.1002/(sici)1099-1085(199610)10:10<1283::aid-hyp460>3.0.co;2-m, 1996.

Slater, A. G., Schlosser, C. A., Desborough, C. E., Pitman, A. J., Henderson-Sellers, A., Robock, A., Vinnikov, K. Y., Entin, J., Mitchell, K., Chen, F., Boone, A., Etchevers, P., Habets, F., Noilhan, J., Braden, H., Cox, P. M., de Rosnay, P., Dickinson, R. E., Yang, Z.-L., Dai, Y.-J., Zeng, Q., Duan, Q., Koren, V., Schaake, S., Gedney, N., Gusev, Y. M., Nasonova, O. N., Kim, J., Kowalczyk, E. A., Shmakin, A. B., Smirnova, T. G., Verseghy, D., Wetzel, P., and Xue, Y.: The Representation of Snow in Land Surface Schemes: Results from PILPS 2(d), Journal of Hydrometeorology, 2, 7–25, https://doi.org/10.1175/1525-7541(2001)002<0007:trosil>2.0.co;2, 2001.

Sproles, E. A., Nolin, A. W., Rittger, K., and Painter, T. H.: Climate change impacts on maritime mountain snowpack in the Oregon Cascades, Hydrology and Earth System Sciences, 17, 2581–2597, https://doi.org/10.5194/hess-17-2581-2013, 2013.

Storck, P.: Trees, snow and flooding: an investigation of forest canopy effects on snow accumulation and melt at the plot and watershed scales in the Pacific Northwest, Tech. rep., Washington State University Department of Civil and Environmental Engineering, https://ir.library.oregonstate.edu/concern/defaults/xk81jr150, 2000.

Strahler, A., Muchoney, D., Borak, J., Friedl, M., Gopal, S., Labin, E., and Moody, A.: MODIS Land Cover Product Algorithm Theoretical Basis Document (ATBD) Version 5.0 MODIS Land Cover and Land-Cover Change, Tech. rep., Boston University, Boston, https://modis.gsfc.nasa.gov/data/atbd/atbd_mod12.pdf, 1999.

Sun, N., Yan, H., Wigmosta, M. S., Leung, L. R., Skaggs, R., and Hou, Z.: Regional Snow Parameters Estimation for Large-Domain Hydrological Applications in the Western United States, Journal of Geophysical Research: Atmospheres, 124, 5296–5313, https://doi.org/10.1029/2018jd030140, 2019.

Sun, S., Jin, J., and Xue, Y.: A simple snow-atmosphere-soil transfer model, 104, 19 587–19 597, https://doi.org/10.1029/1999jd900305, 1999.

Swart, N. C., Cole, J. N. S., Kharin, V. V., Lazare, M., Scinocca, J. F., Gillett, N. P., Anstey, J., Arora, V., Christian, J. R., Hanna, S., Jiao, Y., Lee, W. G., Majaess, F., Saenko, O. A., Seiler, C., Seinen, C., Shao, A., Sigmond, M., Solheim, L., von Salzen, K., Yang, D., and Winter, B.: The Canadian Earth System Model version 5 (CanESM5.0.3), Geoscientific Model Development, 12, 4823–4873, https://doi.org/10.5194/gmd-12-4823-2019, 2019.

Swenson, S. C. and Lawrence, D. M.: A new fractional snow-covered area parameterization for the Community Land Model and its effect on the surface energy balance, Journal of Geophysical Research: Atmospheres, 117, n/a–n/a, https://doi.org/10.1029/2012jd018178, 2012.

Tabler, R. D., Benson, C. S., Santana, B. W., and Ganguly, P.: Estimating snow transport from wind speed records: estimates versus measurements at Prudhoe Bay, Alaska, in: Proceedings of the 58th Annual Western Snow Conference, Sacramento, California, pp. 61–72, Western Snow Conference, sites/westernsnowconference.org/PDFs/1990Tabler.pdf, 1990.

Thomas, G. and Rowntree, P. R.: The Boreal Forests and Climate, Quarterly Journal of the Royal Meteorological Society, 118, 469–497, https://doi.org/10.1002/qj.49711850505, 1992.

https://doi.org/10.5194/tc-2021-319
Preprint. Discussion started: 30 November 2021

Toon, O. B., McKay, C. P., Ackerman, T. P., and Santhanam, K.: Rapid calculation of radiative heating rates and photodissociation rates in inhomogeneous multiple scattering atmospheres, Journal of Geophysical Research, 94, 16 287, https://doi.org/10.1029/jd094id13p16287, 1989.

Trujillo, E., Ramírez, J. A., and Elder, K. J.: Topographic, meteorologic, and canopy controls on the scaling characteristics of the spatial distribution of snow depth fields, Water Resources Research, 43, https://doi.org/10.1029/2006wr005317, 2007.

van den Hurk, B., Kim, H., Krinner, G., Seneviratne, S. I., Derksen, C., Oki, T., Douville, H., Colin, J., Ducharne, A., Cheruy, F., Viovy, N., Puma, M. J., Wada, Y., Li, W., Jia, B., Alessandri, A., Lawrence, D. M., Weedon, G. P., Ellis, R., Hagemann, S., Mao, J., Flanner, M. G., Zampieri, M., Materia, S., Law, R. M., and Sheffield, J.: LS3MIP (v1.0) contribution to CMIP6: the Land Surface, Snow and Soil moisture Model Intercomparison Project – aims, setup and expected outcome, Geoscientific Model Development, 9, 2809–2832, https://doi.org/10.5194/gmd-9-2809-2016, 2016.

van Kampenhout, L., Lenaerts, J. T. M., Lipscomb, W. H., Sacks, W. J., Lawrence, D. M., Slater, A. G., and van den Broeke, M. R.: Improving the Representation of Polar Snow and Firn in the Community Earth System Model, Journal of Advances in Modeling Earth Systems, 9, 2583–2600, https://doi.org/10.1002/2017ms000988, 2017.

Verseghy, D.: CLASS – The Canadian Land Surface Scheme (Version 3.6), Tech. rep., Climate Research Division, Science and Technology Branch, Environment Canada, 2012.

Verseghy, D.: CLASS – The Canadian land surface scheme (v.3.6.2), Tech. rep., Climate Research Division, Science and Technology Branch, Environment Canada, 2017.

Verseghy, D., Cole, J., and Lazare, M.: Canadian Land Surface Scheme including Biogeochemical Cycles (CLASSIC) model snowAlbedoTransmiss.f90 File Reference [code], Tech. rep., https://cccma.gitlab.io/classic/snowAlbedoTransmiss$_8 f90.html$, 2020.

Verseghy, D. L.: Class-A Canadian land surface scheme for GCMS. I. Soil model, International Journal of Climatology, 11, 111–133, https://doi.org/10.1002/joc.3370110202, 1991.

Viterbo, P. and Betts, A. K.: Impact on ECMWF forecasts of changes to the albedo of the boreal forests in the presence of snow, Journal of Geophysical Research: Atmospheres, 104, 27 803–27 810, https://doi.org/10.1029/1998jd200076, 1999.

Voldoire, A., Sanchez-Gomez, E., y Mélia, D. S., Decharme, B., Cassou, C., Sénési, S., Valcke, S., Beau, I., Alias, A., Chevallier, M., Déqué, M., Deshayes, J., Douville, H., Fernandez, E., Madec, G., Maisonnave, E., Moine, M.-P., Planton, S., Saint-Martin, D., Szopa, S., Tyteca, S., Alkama, R., Belamari, S., Braun, A., Coquart, L., and Chauvin, F.: The CNRM-CM5.1 global climate model: description and basic evaluation, Climate Dynamics, 40, 2091–2121, https://doi.org/10.1007/s00382-011-1259-y, 2012.

Voordendag, A., Réveillet, M., MacDonell, S., and Lhermitte, S.: Snow model comparison to simulate snow depth evolution and sublimation at point scale in the semi-arid Andes of Chile, https://doi.org/10.5194/tc-2021-9, 2021.

Wakahama, G.: The metamorphism of wet snow. International Association of Scientific Hydrology Publication 79, in: General Assembly of Bern 1967 – Snow and Ice, p. 370–379, 1968.

Wang, W., Yang, K., Zhao, L., Zheng, Z., Lu, H., Mamtimin, A., Ding, B., Li, X., Zhao, L., Li, H., Che, T., and Moore, J. C.: Characterizing Surface Albedo of Shallow Fresh Snow and Its Importance for Snow Ablation on the Interior of the Tibetan Plateau, Journal of Hydrometeorology, 21, 815–827, https://doi.org/10.1175/jhm-d-19-0193.1, 2020.

Wang, Z. and Zeng, X.: Evaluation of Snow Albedo in Land Models for Weather and Climate Studies, Journal of Applied Meteorology and Climatology, 49, 363–380, https://doi.org/10.1175/2009jamc2134.1, 2010.

Warren, S. G. and Wiscombe, W. J.: A Model for the Spectral Albedo of Snow. II: Snow Containing Atmospheric Aerosols, Journal of the Atmospheric Sciences, 37, 2734–2745, https://doi.org/10.1175/1520-0469(1980)037<2734:amftsa>2.0.co;2, 1980.

https://doi.org/10.5194/tc-2021-319
Preprint. Discussion started: 30 November 2021

Warren, S. G. and Wiscombe, W. J.: Comment on "radiative properties of snow for clear sky solar radiation", Cold Regions Science and Technology, 5, 177–180, https://doi.org/10.1016/0165-232x(81)90053-7, 1981.

Watson, F. G., Anderson, T. N., Newman, W. B., Alexander, S. E., and Garrott, R. A.: Optimal sampling schemes for estimating mean snow water equivalents in stratified heterogeneous landscapes, Journal of Hydrology, 328, 432–452, https://doi.org/10.1016/j.jhydrol.2005.12.032, 2006.

Webster, M., Gerland, S., Holland, M., Hunke, E., Kwok, R., Lecomte, O., Massom, R., Perovich, D., and Sturm, M.: Snow in the changing sea-ice systems, Nature Climate Change, 8, 946–953, https://doi.org/10.1038/s41558-018-0286-7, 2018.

Wigmosta, M. S., Vail, L. W., and Lettenmaier, D. P.: A distributed hydrology-vegetation model for complex terrain, Water Resources Research, 30, 1665–1679, https://doi.org/10.1029/94wr00436, 1994.

Winstral, A., Elder, K., and Davis, R. E.: Spatial Snow Modeling of Wind-Redistributed Snow Using Terrain-Based Parameters, Journal of Hydrometeorology, 3, 524–538, https://doi.org/10.1175/1525-7541(2002)003<0524:ssmowr>2.0.co;2, 2002.

Wiscombe, W. J. and Warren, . S. G.: A Model for the Spectral Albedo of Snow. I: Pure Snow, Journal of the Atmospheric Sciences, 37, 2712–2733, https://doi.org/10.1175/1520-0469(1980)037<2712:amftsa>2.0.co;2, 1980.

Yang, Z.-L. and Niu, G.-Y.: The Versatile Integrator of Surface and Atmosphere processes, 38, 175–189, https://doi.org/10.1016/s0921-8181(03)00028-6, 2003.

Yang, Z.-L., Dickinson, R. E., Robock, A., and Vinnikov, K. Y.: Validation of the Snow Submodel of the Biosphere–Atmosphere Transfer Scheme with Russian Snow Cover and Meteorological Observational Data, Journal of Climate, 10, 353–373, https://doi.org/10.1175/1520-0442(1997)010<0353:votsso>2.0.co;2, 1997.

Zhong, E., Li, Q., Sun, S., Chen, W., Chen, S., and Nath, D.: Improvement of a snow albedo parameterization in the Snow–Atmosphere–Soil Transfer model: evaluation of impacts of aerosol on seasonal snow cover, Advances in Atmospheric Sciences, 34, 1333–1345, https://doi.org/10.1007/s00376-017-7019-0, 2017.

https://doi.org/10.5194/tc-2021-319
Preprint. Discussion started: 30 November 2021

The Cryosphere
Discussions
Open Access
EGU

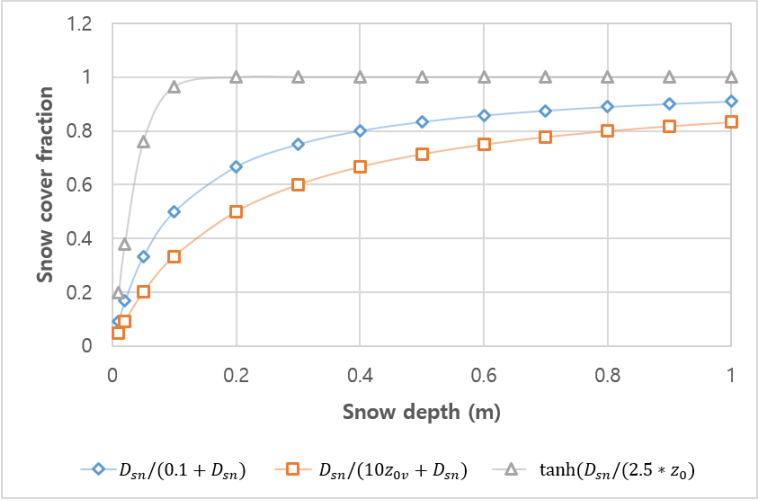

Figure 1. Original (Eq. (d) in Table 2: ground fraction covered by snow, Eq. (e): vegetation fraction covered by snow) and new formulation (Eq. (f): snow cover fraction depending on the surface type) for snow cover fraction in BATS model (Yang et al., 1997) when land cover type is short grass ($z_0 = 0.02$ m).

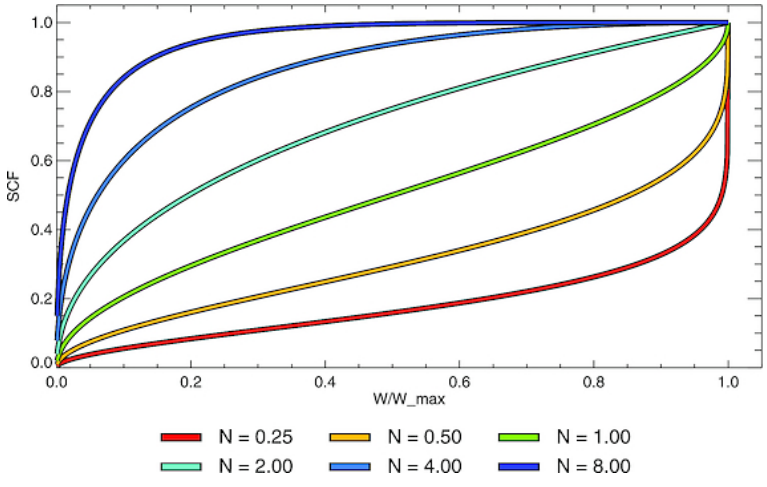

Figure 2. Depletion curves of Snow Cover Fraction (SCF) depending on the shape parameter N_{melt} (from Swenson and Lawrence, 2012, Fig. 9; Copyright 2012 by the American Geophysical Union.). The x-axis is snow depth in meters.

Tables

https://doi.org/10.5194/tc-2021-319
Preprint. Discussion started: 30 November 2021

The Cryosphere
Discussions
Open Access
EGU

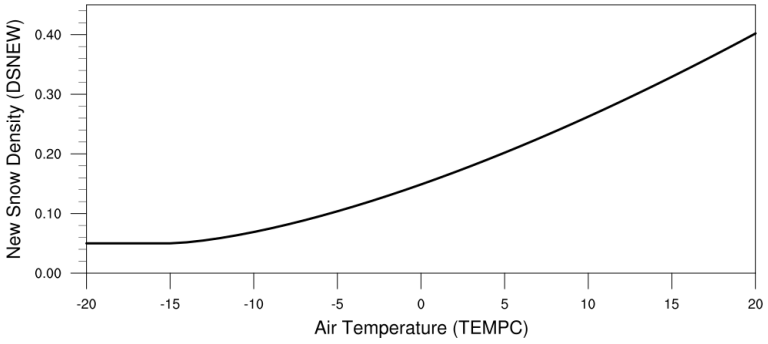

Figure 3. The relationship between the 2 m air temperature (°C) and the new snow density (g m^{-3}) in Noah LSM.

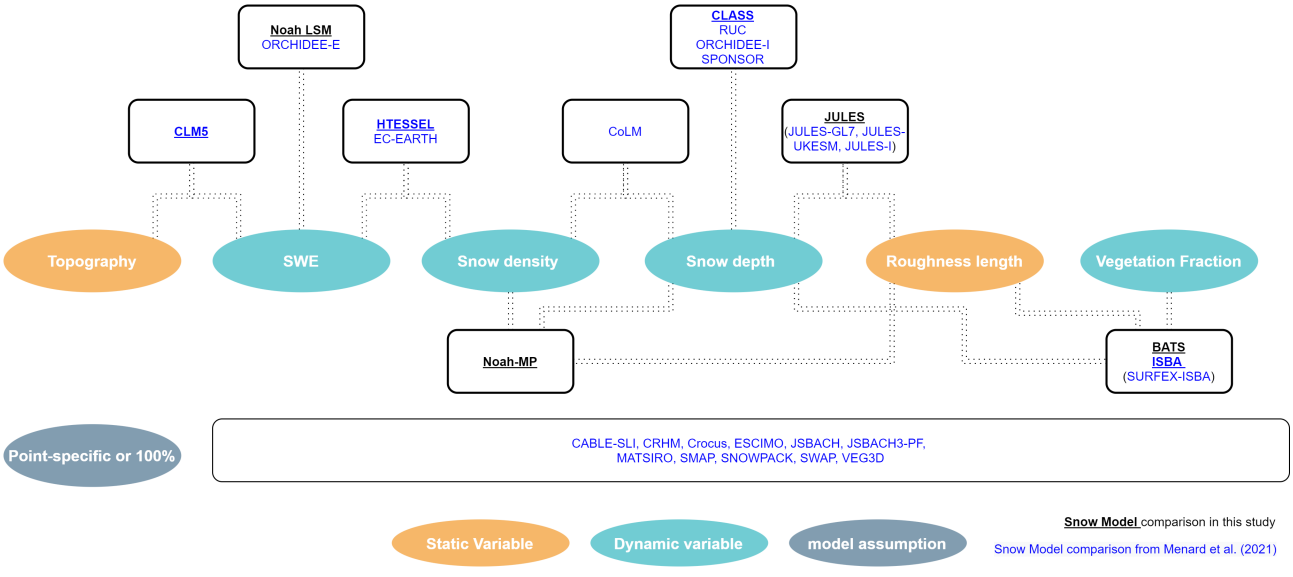

Figure 4. Conceptual diagram key variables of snow cover fraction by snow model intercomparison of this study and the ESM-SnowMIP

https://doi.org/10.5194/tc-2021-319
Preprint. Discussion started: 30 November 2021

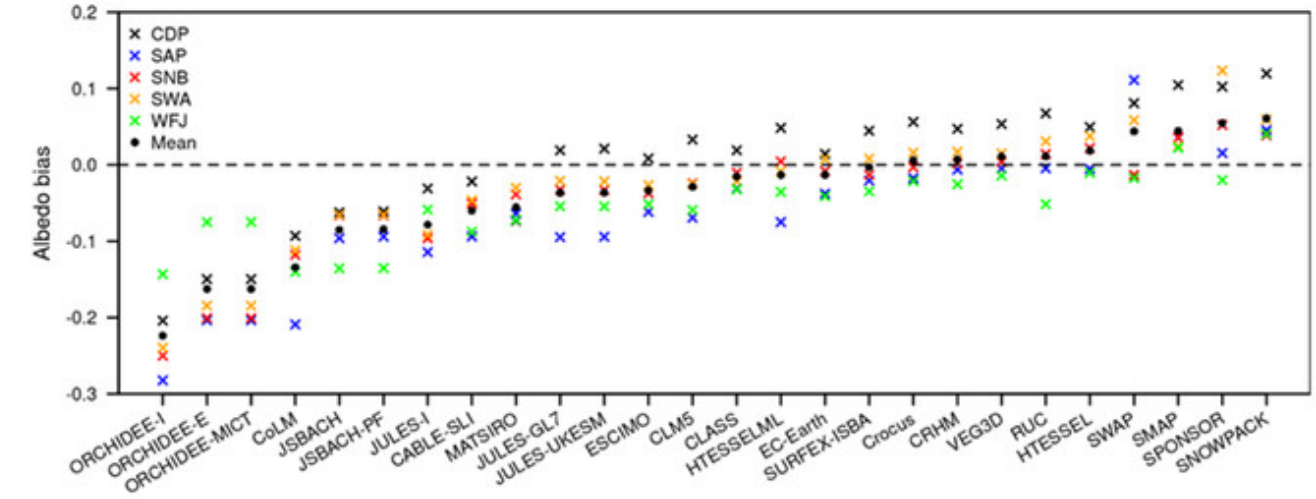

Figure 5. Model ranking by albedo biases from negative to positive (from Menard et al., 2021, part of Fig. 2; Bulletin of the American Meteorological Society 102, 1; 10.1175/BAMS-D-19-0329.1, © American Meteorological Society. Used with permission.). CLASS has the lowest albedo bias among CLM 5, CLASS, and HTESSEL. The site names are abbreviated as follows. CDP = Col de Porte, SAP = Sapporo, RME = Reynolds Mountain East, SNB = Senator Beck, SOD = Sodankylä, SWA = Swamp Angel, and WFJ = Weissfluhjoch.

Table 1. Variables or parameters for parameterization of snow cover in eight LSMs.

Variables or parameters	Land surface model							
	Noah LSM	HTESSEL	BATS	CLASS	Noah-MP	CLM 5	JULES	ISBA
SWE	O	O		O	O	O		
Snow depth			O	O	O		O	O
Snow density		O		O	O			
Thresholds of SWE	O					O		
Thresholds of Snow Depth				O				O
Roughness length			O		O		O	O
Melting Factor					O			
Distribution shape parameter	O							
Consideration of land surface type	O		O			O		
Vegetation fraction			O					O
Consideration of elevation						O		

https://doi.org/10.5194/tc-2021-319
Preprint. Discussion started: 30 November 2021

The Cryosphere Discussions
Open Access
EGU

Table 2. Snow cover parameterization in eight different LSMs.

Land surface model	Expressions	Reference
Noah LSM	(a) $f_s = 1 - \exp(-P_s \frac{W_s}{W_{\max}}) + \frac{W_s}{W_{\max}} \exp(P_s)$	Koren et al. (1999)
HTESSEL	(b) $f_s = \min(1, \frac{W_s}{15})$ (c) $f_s = \min(1, \frac{W_s}{\rho_{sn}} 0.1)$	Dutra et al. (2009)
BATS	(d) $f_{s,g} = D_{sn}/(0.1\mathrm{m} + D_{sn})$ (e) $f_{s,v} = D_{sn}/(10 z_{0v} + D_{sn})$ (f) $f_{s,i} = \tanh \frac{D_{sn}}{2.5 z_0^i}$	Dickinson et al. (1993) Yang et al. (1997)
CLASS	(g) $f_s = D_{sn}/D_{sn,lim}$ (h) $D_{sn} = \frac{W_s}{\rho_{sn}}$ (i) $f_s = 1 - 0.01(15 - 100 D_{sn})^{1.7}$	Verseghy (2012) Brown et al. (2003)
Noah-MP	(j) $f_s = tanh(D_{sn}/2.5 z_0 F_{melt})$ (k) $F_{melt} = (\rho_{sn}/100)^M$ (l) $\rho_{sn} = \frac{S}{D_{sn}}$	Niu and Yang (2007)
CLM 5	(m) $f_s^{n+1} = 1 - [(1 - \tanh(k_{accum} q_{snow} \Delta t))(1 - f_s^n)]$ (n) $f_s = 1 - [\frac{1}{\pi} acos(2 \frac{W_s}{W_{\max}} - 1)]^{N_{melt}}$ (o) $N_{melt} = \frac{200}{\max(10, \sigma_{topo})}$	Lawrence et al. (2018)
JULES	(p) $f_s = D_{sn}/(10 z_0 + D_{sn})$	Best et al. (2011)
ISBA	(q) $f_{s,g} = \min(1, D_{sn}/D_{sn,lim})$ (r) $f_{s,v} = D_{sn}/(2 z_{0v} + D_{sn})$	Decharme et al. (2016)

Symbols: f_s :fractional snow coverage; P_s: distribution shape parameter; W_s: snow water equivalent; $W_{\max}$: threshold SWE above which f_s is 100%; ρ_{sn}: snow density; $f_{s,g}$: fraction of ground covered by snow; D_{sn}: snow depth; $f_{s,v}$: fraction of vegetation covered by snow; z_{0v}: roughness length on vegetated area; $f_{s,i}$: snow cover fraction depending on surface type, ex) bare soil or grass; z_0^i: roughness length depending on surface type; $D_{sn,lim}$: maximum limit of snow depth above which f_s is 100%; z_0: the ground roughness length (m) ($z_0 = 0.01$ m in the Noah-MP); F_{melt}: melting factor for snow cover fraction; M: melting factor determining the curves in melting season ($M = 1.0$ in the Noah-MP, a larger value for a larger scale generally); S: snow mass (kg m^{-2});f_s^{n+1}: updated snow cover fraction; f_s^n: snow cover fraction from the previous time step; k_{accum}: a constant (default value = 0.1); $q_{snow}\Delta t$: amount of new snow; N_{melt}: parameter that depends on the topographic variability within the grid cell; σ_{topo}: standard deviation of the elevation within a grid cell calculated from a high resolution DEM (1 km DEM is used for CLM 5)

https://doi.org/10.5194/tc-2021-319
Preprint. Discussion started: 30 November 2021

Table 3. Typical ranges for surface albedo (Armstrong and Brun, 2008).

Snow condition and land surface types	Surface albedo
Fresh, dry snow	0.80–0.95
Old, dry snow	0.70–0.80
Wet snow	0.50–0.70
Melting ice/snow	0.25–0.80
Snow-covered forest	0.25–0.40
Snow-free vegetation/soil	0.10–0.30
Water (high solar elevation)	0.05–0.10

https://doi.org/10.5194/tc-2021-319
Preprint. Discussion started: 30 November 2021


The Cryosphere Discussions
Open Access
EGU

Table 4. Variables considered for snow albedo parameterization in eight LSMs.

Variables or parameters	Land surface model						
	Noah LSM	HTESSEL	BATS*	CLASS*	CLM 5	JULES**	ISBA
Separate direct and diffuse albedo			O		O	O	
Separate visible and near-infrared area			O	U	O	O	O
Thresholds of SWE				O			
Thresholds of Snow depth						V	
Snow depth						V	
Fresh snowfall rate				O		O	
Snow cover fraction	O				O	O	
Consideration of vegetation effects (land surface type)	O	O	O		O	V	
Solar zenith angle			O		O	O	
Black carbon, mineral dust, organic carbon			O		O		
Ice grain size			O		O	O	O
Age of the first snow layer							O
Near surface atmospheric pressure							O
Melting snow and dry snow				U			
Surface temperature						V	

*Noah-MP has two options for snow albedo parameterization from BATS or CLASS. Especially, CLASS is updated (U) for CLASSIC earth system model. **JULES has two snow albedo options, the diagnostic scheme (V) and the prognostic albedo scheme (O).

https://doi.org/10.5194/tc-2021-319
Preprint. Discussion started: 30 November 2021

The Cryosphere Discussions
Open Access
EGU

Table 5. Snow albedo parameterization in eight different LSMs.

Land surface model	Expressions	Reference
Noah LSM	(a) $\alpha = \alpha_0 + f_s(\alpha_{sn} - \alpha_0)$ (b) $\alpha = \alpha_0 + (1-\sigma_f) f_s(\alpha_{sn} - \alpha_0)$ (c) $\alpha_{\max} = \alpha_{\max,sat} + C(\alpha_{\max,CofE} - \alpha_{\max,sat})$ (d) $\alpha_{sn} = \alpha_{\max} * A^{t^B}$	Livneh et al. (2010)
HTESSEL	(e) $\alpha_{sn}^{t+1} = \begin{cases} \alpha_{sn}^t - \gamma_a \Delta t/\gamma_1 & M_{sn} = 0 \\ \left(\alpha_{sn}^t - \alpha_{\min,H}\right)\exp\left(-\gamma_f \Delta t/\gamma_1\right) + \alpha_{\min,H} & M_{sn} > 0 \text{ or } T_{sn} \geq T_f - 2 \end{cases}$ (f) $\alpha_{sn}^{t+1} = \alpha_{sn}^t + \min(1, \frac{F\Delta t}{10})(\alpha_{\max,H} - \alpha_{sn}^t)$	Dutra et al. (2009)
BATS	(g) $\alpha_{sn,vis} = 0.95 * (1 - 0.2 * F_{age})$ (h) $\alpha_{sn,nir} = 0.65 * (1 - 0.5 * F_{age})$ (i) $\alpha_{sn,vis}^{\mu} = \alpha_{sn,vis} + 0.4 * F_{zenith} * (1 - \alpha_{sn,vis})$ (j) $\alpha_{sn,nir}^{\mu} = \alpha_{sn,nir} + 0.4 * F_{zenith} * (1 - \alpha_{sn,nir})$	Dickinson et al. (1993)
CLASS	(k) $\alpha_{sn}^{t+1} = \alpha_{sn}^t + \min(1, \frac{F\Delta t}{W_{\max}})(\alpha_{\max} - \alpha_{sn}^t)$ (l) $\alpha_{sn}^t = 0.55 + (\alpha_{sn}^{t-1} - 0.55) * \exp(\frac{-0.01*\Delta t}{3600})$ (m) $\alpha_{sn,total}^t = \alpha_{sn,total,old} + (\alpha_{sn}^{t-1} - \alpha_{sn,total,old}) * \exp(\frac{-0.01*\Delta t}{3600})$ (n) $\alpha_{sn,vis} = 0.7857\alpha_{sn,total} + 0.29$ (o) $\alpha_{sn,nir} = 1.2142\alpha_{sn,total} - 0.29$ (p) $\alpha_{sn,vis} = 0.9706\alpha_{sn,total} + 0.1347$ (q) $\alpha_{sn,nir} = 1.0294\alpha_{sn,total} - 0.1347$	Verseghy et al. (2012) Melton et al. (2019)
CLM 5	(r) $\alpha_{g,\Lambda}^{\mu} = \alpha_{soil,\Lambda}^{\mu}(1 - f_s) + \alpha_{sno,\Lambda}^{\mu} f_s$ (s) $\alpha_{g,\Lambda} = \alpha_{soil,\Lambda}(1 - f_s) + \alpha_{sno,\Lambda} f_s$ (t) $\alpha_{soil,vis}^{\mu} = \alpha_{soil,vis} = 0.6$ (u) $\alpha_{soil,nir}^{\mu} = \alpha_{soil,nir} = 0.4$ (v) $\alpha_{soil,\Lambda}^{\mu} = \alpha_{soil,\Lambda} = 0.05(\mu + 0.15)^{-1}$ (w) $\alpha_{soil,\Lambda}^{\mu} = \alpha_{soil,\Lambda} = (\alpha_{sat,\Lambda} + \Delta) \leq \alpha_{dry,\Lambda}$	Lawrence et al. (2018)

Symbols: α: albedo; α_0: snow free albedo; α_{sn}: snow albedo; f_s: fractional snow coverage; σ_f: green vegetation fraction ($0 \leq \sigma_f \leq 1$); $\alpha_{\max}$: maximum albedo value of fresh fallen snow; $\alpha_{\max,sat}$: satellite-based maximum snow albedo; C: proportionality coefficient (0.5); $\alpha_{\max,CofE}$: maximum snow albedo from U.S. Army Corps of Engineers (1956) (0.85); A: 0.95 for accumulation phase and 0.58 for ablation phase; B: 0.82 for accumulation phase and 0.46 for ablation phase; t: number of days since the last snowfall; α_{sn}^{t+1}: snow albedo at the next time step; α_{sn}^t: snow albedo at the current time step; γ_a: linear coefficient for decrease of albedo of non-melting snow (γ_a=0.008); Δt: model time step; γ_1: length of day (γ_1=86400); M_{sn}: melting snow amount; $\alpha_{\min,H}$: minimum albedo of exposed snow ($\alpha_{\min,H}$=0.5 for HTESSEL); γ_f:coefficient for exponential decrease of snow density and melting snow albedo; T_{sn}: snow temperature (K); T_f: freezing temperature (T_f=273.16 K); F: mass fluxes of snowfall (kg m^{-2}s^{-1}); $\alpha_{\max,H}$: maximum albedo of exposed snow ($\alpha_{\max,H}$=0.85 for HTESSEL); $\alpha_{sn,vis}$: diffuse snow albedo for visible area; $\alpha_{sn,nir}$: diffuse snow albedo for near-infrared area; F_{age}: factor to account for snow aging; $\alpha_{sn,vis}^{\mu}$: direct beam snow albedo for visible area; $\alpha_{sn,nir}^{\mu}$: direct beam snow albedo for near-infrared area; F_{zenith}: factor to account for solar zenith angle impact; $\alpha_{sn,total}^t$: total snow albedo at the current time step; $\alpha_{sn,total}$: total snow albedo for visible and near-infrared area; $\alpha_{sn,total,old}$: set to a value of 0.5 for melting snow, 0.7 for dry snow; $\alpha_{g,\Lambda}^{\mu}$: direct beam ground albedo; $\alpha_{soil,\Lambda}^{\mu}$: direct beam soil albedo; $\alpha_{sno,\Lambda}^{\mu}$: direct beam snow albedo; $\alpha_{g,\Lambda}$: diffuse ground albedo; $\alpha_{soil,\Lambda}$: diffuse soil albedo; $\alpha_{sno,\Lambda}$: diffuse snow albedo; $\alpha_{soil,vis}^{\mu}$: direct beam soil albedo for visible area; $\alpha_{soil,vis}$: diffuse soil albedo for visible area; $\alpha_{soil,nir}^{\mu}$: direct beam soil albedo for near-infrared area; $\alpha_{soil,nir}$: diffuse soil albedo for near-infrared area; μ: cosine of the solar zenith angle; $\alpha_{sat,\Lambda}$: saturated soil albedo; $\alpha_{dry,\Lambda}$: dry soil albedo

https://doi.org/10.5194/tc-2021-319
Preprint. Discussion started: 30 November 2021

Table 5. (Continued).

Land surface model	Expressions	Reference
JULES	(x1) $\alpha_{sn} = \alpha_{cds} + k_1(\alpha_0 - \alpha_{cds})(T_g - T_c)$ (x2) $\alpha = \alpha_0 + (\alpha_{sn} - \alpha_0)(1 - e^{-D_{sn}/D_m})$ (y1) $\alpha_{vis} = 0.98 - 0.002(r^{1/2} - r_0^{1/2})$ (y2) $\alpha_{nir} = 0.7 - 0.09ln(r/r_0)$	Best et al. (2011)
ISBA	(z1) $\alpha_{\mathrm{sn}}(1) = \max\left[0.6, \min\left(0.92, 0.96 - 1.58\sqrt{d_{\mathrm{opt}}(1)}\right)\right.$ $\left. - \min\left(1, \max\left(\frac{1}{2}, \frac{P_{\mathrm{a}}}{P_{\mathrm{ref}}}\right)\right) \times 0.2\frac{A_{\mathrm{sn}}(1)}{A_{\mathrm{ref}}}\right]$ (z2) $\beta_{\mathrm{sn}}(1,i) = \max\left[40, 0.00192\rho_{\mathrm{s}}(i)/\sqrt{d_{\mathrm{opt}}(i)}\right]$ (z3) $\alpha_{\mathrm{sn}}(2) = \max\left[0.3, 0.9 - 15.4\sqrt{d_{\mathrm{opt}}(1)}\right]$ (z4) $\beta_{\mathrm{sn}}(2,i) = \max\left[100, 0.01098\rho_{\mathrm{s}}(i)/\sqrt{d_{\mathrm{opt}}(i)}\right]$ (z5) $\alpha_{\mathrm{sn}}(3) = 0.88 + 346.2d' - 32.31\sqrt{d'}$ with $d' = \min\left[0.0023, d_{\mathrm{opt}}(i)\right]$ (z6) $\beta_{\mathrm{sn}}(3,i) = +\infty$	Decharme et al. (2016)

Symbols: α: albedo; α_0: snow free albedo; α_{sn}: snow albedo; α_{cds}: cold deep snow albedo; k_1: snow aging parameter; T_g: surface temperature; T_c: snow albedo threshold temperature; D_{sn}: snow depth; D_m: surface masking snow depth; α_{vis}: snow albedo for visible area; α_{nir}: snow albedo for near-infrared area; r: grain size; r_0: fresh snow grain size ($r_0 = 50\ \mu m$);$\mathrm{d_{opt}}(i)$: optical diameter of snow in each layer i; P_{a}: near surface atmospheric pressure; P_{ref}: reference pressure, 870 hPa; A_{sn}: age of the first snow layer expressed in days; A_{ref}: reference age of snow decreasing due to impurities, 60 days; $\rho_{\mathrm{s}}(i)$: snow density in ith layer

Table 6. Typical albedo values for fresh snow, old dry snow, and melting snow in CLASS model (Verseghy et al., 2020).

Snow characteristics	Total albedo	Visible albedo	Near-infrared albedo
Fresh snow	0.84	0.95	0.73
Old dry snow	0.70	0.84	0.56
Melting snow	0.50	0.62	0.38

https://doi.org/10.5194/tc-2021-319
Preprint. Discussion started: 30 November 2021

The Cryosphere Discussions
Open Access
EGU

Table 7. Variables considered for snow density and snow depth parameterization.

Variables or parameters	Land surface model							
	Noah LSM	HTESSEL	BATS	CLASS	Noah-MP	CLM 5	JULES	ISBA
Air temperature	N	N			N	N		N
Snow temperature							T	S
Wind speed		N				N		N, T
Snow cover fraction		D				D		
SWE	D	D	D	D				
Snowfall rate					D	D		
Liquid water content							T	S
Ice content							T	S
Snow depth				T				V
Snow density	D	D	D	D, T	D	D	T	V, S
Ice grain size			T					
Snow viscosity							T	T
Vertical stress							T	T
Dust, soot			T					

Different symbols, N / T / V / S / D stands for considering variables for parameterizing New snow density / Snow density depending on time / Vertical Stress / Snow viscosity / Snow depth, respectively.

https://doi.org/10.5194/tc-2021-319
Preprint. Discussion started: 30 November 2021

The Cryosphere Discussions
Open Access
EGU

Table 8. Snow density parameterization in eight different LSMs.

Land surface model	Expressions	Reference
Noah LSM	(a) $\Delta Z_{\text{sno}} = \frac{W_s}{\rho_{sn}}$ (b) $\rho_{sn} = \left\{ \begin{array}{ll} 0.05 + 0.0017\,(T_{2m} + 15)^{1.5}, & -15 < T_{2m} \\ \rho_{sn} = 0.05, & T_{2m} \leq -15 \end{array} \right\}$	Gottlib (1980); Koren et al. (1999)
HTESSEL	(c) $D_{sn} = \frac{S}{\rho_{sn} * f_s}$ (d) $\rho_{sn} = a_{sn} + b_{sn}(T_{\text{atm}} - T_f) + c_{sn}(V_a)^{1/2}$	Dutra et al. (2009)
BATS	(e) $D_{sn} = \frac{S}{\rho_{sn}}$ (f) $\rho_{sn} = 0.1 + 0.3F_{AGE}$	Dickinson et al. (1993); Wang et al. (2020)
CLASS	(g) $D_{sn} = \frac{W_s}{\rho_{sn}}$ (h) $\rho_s(t+1) = [\rho_s(t) - \rho_{s,\max}] \exp\left[-\frac{0.01\Delta t}{3600}\right] + \rho_{s,\max}$ (i) $\rho_{s,\max} = A_s - \left[\frac{204.70}{D_{sn}}\right]\left[1.0 - \exp\left(\frac{-D_{sn}}{0.673}\right)\right]$	Verseghy et al. (2012) Brown et al. (2003)
Noah-MP	(j) $D_{zs} = \frac{P_{sg}}{BD_{fall}}$ (k) $BD_{fall} = \left\{ \begin{array}{ll} 120 & 120 > \rho_{sn} \\ \rho_{sn} & 120 < \rho_{sn} \end{array} \right\}$ (l) $\rho_{sn} = 67.92 + 51.25e^{\frac{\left(T_{\text{atm}} - T_f\right)}{2.59}}$	Yang et al., (2011)
CLM 5	(m) $\Delta z_{sno} = \frac{q_{grnd,ice}\Delta t}{f_s \rho_{sn}}$ (n) $\rho_{sn} = \rho_T + \rho_w$ (o) $\rho_T = \left\{ \begin{array}{ll} 50 + 1.7(17)^{1.5}, & T_{\text{atm}} > T_f + 2 \\ 50 + 1.7\,(T_{\text{atm}} - T_f + 15)^{1.5}, & T_f - 15 < T_{\text{atm}} \leq T_f + 2 \\ -3.833\,(T_{\text{atm}} - T_f) - 0.0333\,(T_{\text{atm}} - T_f)^2, & T_{\text{atm}} \leq T_f - 15 \end{array} \right\}$ (p) $\rho_W = 266.861\left(\frac{1+\tanh\left(\frac{W_{atm}}{5}\right)}{2}\right)^{8.8}$	Anderson et al. (1976); Lawrence et al. (2018); van Kampenhout et al. (2017)
JULES	(q) $\frac{\delta \rho_k}{\delta t} = \frac{\rho_k g M_k}{\eta_0} \exp\left(\frac{k_s}{T_m} - \frac{k_s}{T_k} - \frac{\rho_k}{\rho_0}\right)$	Best et al. (2011)
ISBA	(r) $\frac{\partial \rho_{\text{sn}}(i)}{\partial t} = \rho_{\text{sn}}(i)\frac{\sigma(i)}{\eta(i)} + \max\left(0, \frac{\rho_{\text{W max}} - \rho_{\text{sn}}(i)}{\tau_{\text{W}}(i)}\right)$ (s) $\sigma(1) = \frac{g\Delta z(1)\rho_{\text{sn}}(1)}{2}$ (t) $\sigma(i) = g\sum_{j=1}^{i-1}\left[\Delta z(j)\rho_{\text{sn}}(j)\right] \quad \forall i > 1$ (u) $\eta(i) = \frac{\eta_0}{f_{\text{W}}(i)}\frac{\rho_{\text{sn}}(i)}{\rho_0}\exp\left(a_\eta \times \min\left(\Delta T_\eta, T_{\text{f}} - T_{\text{sn}}(i)\right) + b_\eta \rho_{\text{sn}}(i)\right)$ (v) $f_{\text{W}}(i) = 1 + 10 \times \min\left(1.0, \frac{W_l(i)}{W_{l\,\max}(i)}\right)$	Decharme et al. (2016)

Symbols: ΔZ_{sno}: new snow depth; W_s: snow water equivalent; ρ_{sn}: new snow density; T_{2m}: 2m temperature; D_{sn}: snow depth (m) ; S: snow mass (kg m^{-2});f_s: snow cover fraction; V_a: the near surface wind speed (ms^{-1});T_{atm}: atmospheric temperature (K); T_f: freezing temperature of water (K); F_{AGE}: snow age factor; $\rho_{s,\max}$: maximum snow density; A_s: empirical constant; P_{sg}: snow on the ground; BD_{fall}: bulk density snowfall; 10 m wind speed; $q_{grnd,ice}$: rate of solid precipitation reaching the ground; Δt: model time step; ρ_T: new snow density of temperature dependent term; ρ_W: new snow density of wind dependent term; W_{atm}: wind speed; ρ_k: density of the k-th snow layer; ρ_0: reference snow density; M_k: the mass of snow above the middle of the layer; T_{m}: temperature of the melting point for water; T_k: temperature of the k-th snow layer; η_0: compactive viscosity; $\rho_{\text{sn}}(i)$: snow density in each layer; g: acceleration of gravity; $\sigma(i)$: vertical stress in each layer; Δz: snow depth changes per time step; $\eta(i)$: snow viscosity in each layer; $T_{sn}(i)$: snow temperature in i-th layer; $\rho_{\text{W max}}$: maximum snow density; $\tau_{\text{W}}(i)$: wind-driven compaction rate in each layer; $f_{\text{W}}(i)$: the decrease of viscosity in the presence of liquid water; $W_{l\,\max}(i)$: maximum liquid-water-holding capacity; $W_l(i)$: liquid water content in i-th layer

https://doi.org/10.5194/tc-2021-319
Preprint. Discussion started: 30 November 2021


The Cryosphere Discussions
Open Access
EGU

Table 9. Spatial variability of snow depth and related processes and predictors (from Clark et al., 2011, Table 2; Copyright 2011 by the American Geophysical Union.).

Process	Predictors	Spatial Scale (m)	References
Variability in microtopography	-	1	Watson et al. (2006)
Snow interception/sublimation from the forest canopy	distance from trunk; spacing of trees; leaf area index	10	Faria et al. (2000); Pomeroy et al. (2002)
Trapping of snow by tall shrubs	vegetation type	changeable	Essery and Pomeroy (2004); McCartney et al. (2006); Pomeroy et al. (2006)
Preferential deposition of snow in sheltered areas and scouring and redeposition of snow by wind	sheltering indices	10–100	Shook and Gray (1996); Lapena and Martz (1996); Luce et al. (1998); Winstral et al. (2002); Anderton et al. (2004); Erickson et al. (2005); Trujillo et al. (2007)
Sloughing and avalanching	slope	10–1000[a]	Elder et al. (1991); Blöschl and Kirnbauer (1992)
Variability in freezing levels	elevation	100–1000[b]	Blöschl and Kirnbauer (1992); Elder et al. (1998); Balk and Elder (2000); Winstral et al. (2002); Marchand and nund Killingtveit (2005) Watson et al. (2006)
Variability in melt energy	elevation; slope; aspect; radiation loading	50–1000	Elder et al. (1991); Luce et al. (1998); Balk and Elder (2000); Watson et al. (2006)

[a] The horizontal scale associated with sloughing and avalanching is often much smaller than the vertical scale.
[b] The horizontal scale associated with variability in freezing levels is often much larger than the vertical scale.